

Master's Programme in Chemical, Biochemical and Materials Engineering

Improvement of a fractionation simulation

Santeri Haapanen

Copyright © 2024 Santeri Haapanen

Author Santeri Haapanen

Title Improvement of a fractionation simulation

Degree programme Chemical, Biochemical and Materials Engineering

Major Chemical and Process Engineering

Supervisor Prof. Ville Alopaeus

Advisor Risto Honkanen (MSc)

Collaborative partner ANDRITZ Oy

Date 18 July 2024

Number of pages 65+5

Language English

Abstract

A part of the biomethanol purification process of ANDRITZ was simulated on CHEMCAD and Aspen Plus. The goal of the thesis was to investigate how to improve the accuracy of the process simulation by choosing the correct thermodynamic models and by updating the binary interaction parameters (BIPs) of component pairs. The simulations were first run with BIPs found from the databases of CHEMCAD and Aspen. Some of the missing parameters were then updated with values obtained from literature, data regression and UNIFAC estimations and their effects were studied. The BIPs for the component pairs water/methanol–DMS/DMDS/terpenes had the biggest impact on the results due to the formation of minimum boiling heterogeneous azeotropes which increased the volatility of the compounds. Finally, sensitivity analyses were conducted to study the effects of varying process conditions. Increasing the temperature of the sulphur column condenser could increase the separation of DMDS at the cost of lower methanol yield. Turpentine separation in decantation increased with increasing turpentine concentration in the feed. Methanol yield could be maximised by increasing the steam flow into the methanol column.

Keywords biomethanol, purification, distillation, simulation, phase equilibrium

Tekijä Santeri Haapanen

Työn nimi Erotteluprosessin simuloinnin kehittäminen

Koulutusohjelma Kemian-, bio- ja materiaalitekniikka

Pääaine Kemian- ja prosessitekniikka

Työn valvoja Prof. Ville Alopaeus

Työn ohjaaja DI Risto Honkanen

Yhteistyötaho ANDRITZ Oy

Päivämäärä 18.7.2024

Sivumäärä 65+5

Kieli englanti

Tiivistelmä

Osa ANDRITZin biometanolin puhdistusprosessista simuloitiin CHEMCAD- ja Aspen Plus -ohjelmilla. Diplomityön tavoitteena oli tutkia, miten prosessisimulaation tarkkuutta voisi kehittää valitsemalla oikeat termodynaamiset mallit ja päivittämällä komponenttiparien binäärivuorovaikutusparametreja. Simuloinnit ajettiin ensin käyttäen binäärivuorovaikutusparametreja, jotka löytyivät CHEMCADin ja Aspenin tietokannoista. Osa puuttuvista parametreista päivitettiin kirjallisuuden, regressoinnin ja UNIFACin avulla, ja päivitettyjen parametrien vaikutuksia tutkittiin. Suurin vaikutus lopputuloksiin oli vesi/metanoli–DMS/DMDS/tärpätti-parien vuorovaikutusparametreilla, joka johtui heterogeenisten matalan kiehumispisteen omaavien atseotrooppien muodostumisesta, mikä kasvatti kyseisten komponenttien haihtuvuutta. Lopuksi muuttuvien prosessiolosuhteiden vaikutuksia tutkittiin herkkyysanalyysillä. Rikkikolonnin lauhduttimen lämpötilan nostaminen lisäisi DMDS:n erottumista, mutta laskisi metanolin saantoa. Tärpätin erottuvuus lisääntyi dekantoinnissa tärpätin konsentraation kasvaessa syöttövirrassa. Metanolin saanto voitaisiin maksimoida kasvattamalla höyryn virtausta metanolikolonniin.

Avainsanat biometanoli, puhdistus, tislauk, simulointi, faasitasapaino

Preface

This Master's Thesis was done in collaboration with ANDRITZ Oy. Firstly, I'd like to thank my supervisor Professor Ville Alopaeus and advisor MSc Risto Honkanen for their help and guidance. I also want to thank Pia Kyllönen, Henni Kuokka and Nikolas Tolvanen for their important advice and comments.

A big thank you also goes to my friends for the great experiences during these five years at Aalto. Finally, I wish to thank my family for the support throughout my studies.

Otaniemi, 18 July 2024

Santeri Haapanen

Contents

Abstract	3
Abstract (in Finnish)	4
Preface	5
Contents	6
Symbols and abbreviations	8
1 Introduction	9
2 Literature review	10
2.1 Process description	10
2.1.1 Formation of methanol and impurities in pulping	10
2.1.2 Methanol segregation and liquefaction	11
2.1.3 Impurities in crude methanol	12
2.1.4 Crude methanol purification	14
2.2 Thermodynamic models for phase equilibrium modelling	18
2.3 Steady-state simulation in CHEMCAD and Aspen Plus	21
2.3.1 Simulation of distillation	22
2.3.2 Simulation of extraction	23
2.4 Equilibrium data for crude methanol	23
2.4.1 Vapour-liquid and liquid-liquid equilibrium	23
2.4.2 Prediction of lacking experimental data	24
2.5 Electrolyte models	26
3 Simulation of the methanol purification process	28
3.1 Selection of required compounds in methanol purification	28
3.2 Prediction of lacking equilibrium data	29
3.3 Setting up the simulations	31
3.3.1 Acid mixing tank	31
3.3.2 Decanters	32
3.3.3 Columns	32
4 Simulation results	33
4.1 Comparison of CHEMCAD and Aspen Plus simulations	33
4.1.1 Acid mixing tank	33
4.1.2 The first decanter	33
4.1.3 Sulphur column	34
4.1.4 The second decanter	35
4.1.5 Methanol column	35
4.2 Effects of regressed binary interaction parameters	38
4.2.1 Sulphur column	39

4.2.2	Methanol column	41
4.3	Comparison of decantation simulation results to experimental data	43
5	Sensitivity analyses	46
5.1	TRS compounds	46
5.2	Turpentine	48
5.3	Alpha-terpineol and guaiacol	50
5.4	Condenser temperature of the sulphur column	51
5.5	Steam flow into the methanol column	53
6	Conclusions and suggestions for the future	56
	References	57
A	Simulation flowsheets	66
B	Phase equilibrium diagrams	68

Symbols and abbreviations

Symbols

$E_{i,j}^M$	Murphree stage efficiency
G^E	Gibbs energy
K	vapour-liquid distribution ratio
P	pressure of the system
$P_{i,sat}$	saturation pressure of component i
q_i	area parameter of component i in the UNIQUAC model
r_i	volume parameter of component i in the UNIQUAC model
T	temperature
x_i	liquid mole fraction of component i
y_i	vapour mole fraction of component i
α_{ij}	non-randomness parameter in the NRTL model
γ_i	activity coefficient of component i

Abbreviations

BIP	binary interaction parameter
CC	CHEMCAD
COSMO-RS	conductor-like model for real solvents
DMDS	dimethyl disulphide
DMS	dimethyl sulphide
e-NRTL	electrolyte NRTL
EOS	equation of state
EtOH	ethanol
HOC	Hayden-O'Connell equation of state
LLE	liquid-liquid equilibrium
MeOH	methanol
ML	machine learning
MM	methyl mercaptan
NIST	National Institute of Standards and Technology
NRTL	non-random two-liquid model
RMSPE	root mean square percentage error
RR	reflux ratio
SOG	stripper off gas
TRS	total reduced sulphur
UNIFAC	UNIQUAC functional-group activity coefficients model
UNIQUAC	universal quasichemical model
VLE	vapour-liquid equilibrium
VLLE	vapour-liquid-liquid equilibrium
WBL	weak black liquor

1 Introduction

Methanol is an important raw material in the chemical industry. It is primarily used as a feedstock or solvent with common applications including the production of formaldehyde, acetic acid and several other chemicals. It can be utilised as a fuel on its own or mixed with traditional gasoline. [1] In addition, methanol can be used in the transesterification process to produce biodiesel from fatty acids [2].

Green methanol from renewable processes can be split into biomethanol, which is produced from biomass, and e-methanol which is produced from carbon dioxide and green hydrogen. Around 100 Mt of methanol is produced yearly, and the global consumption of methanol is expected to rise to 120 Mt/year by 2025 and to 500 Mt/year by 2050. In 2021, only 0.2 Mt of the product was green methanol, with the main source being biomass gasification. However, the shares of e-methanol and biomethanol in the total production are expected to rise up to around 50 and 27 % respectively by 2050 due to the transition away from fossil fuels. For example, the RED II directive in the European Union states that 14 % of the energy used in transport should come from renewable sources by 2030. [3] Therefore, the interest in green methanol has grown, and new production processes are developed to exploit its potential.

This work focuses on the simulation of a purification process patented by ANDRITZ that produces biomethanol from foul condensate formed in kraft pulping. The goal was to model the process as accurately as possible. An accurate simulation model is an important tool in process design. It ensures that equipment can be sized correctly, and it helps to study the profitability of the process accurately. Improved estimation accuracy also decreases project risks and design margins.

The literature review looks into methanol formation in pulping and different biomethanol purification processes at pulp mills. Additionally, the modelling and simulation of distillation and extraction in CHEMCAD and Aspen Plus are discussed. The simulation results from the two programs are compared in the applied part, and the effects of regressed binary interaction parameters (BIPs) are covered. Finally, sensitivity analyses are conducted to analyze the effects of varying different process conditions to find operating regions for the process.

2 Literature review

This section gives an overview of the available literature on methanol formation in pulping and its purification. Different purification processes are compared and the modelling and simulation of distillation and extraction systems are discussed. Additionally, a summary of experimental equilibrium data regarding the components in crude methanol is presented.

2.1 Process description

The kraft process, invented in 1879, is the most prevailing pulping method [4]. The formation of methanol and its purification at kraft pulp mills are discussed in this section. An overview of the kraft process is presented in Figure 1.

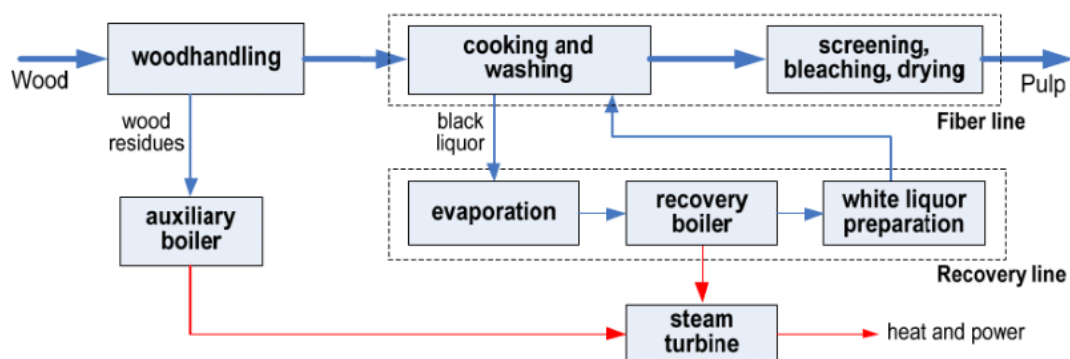


Figure 1: Simplified process diagram of kraft pulping [5].

2.1.1 Formation of methanol and impurities in pulping

Foul condensates are produced in digesters and evaporators in the kraft pulping process [6]. The purpose of digesters is to separate cellulose from lignin by washing the wood chips with white liquor which consists mainly of sodium hydroxide and sodium sulphide. The solution is then washed, and the separated liquid, called black liquor, is sent to the evaporators. The washed pulp continues on the fiber line to be screened, bleached and dried. [5]

The condensates contain pollutants, such as methanol, turpentine and total reduced sulphur compounds (TRS). [6] TRS are one of the main atmospheric emissions at kraft mills and they are known for causing odour problems even at low concentrations. They include hydrogen sulphide (H_2S), dimethyl sulphide (DMS), dimethyl disulphide (DMDS) and methyl mercaptan (MM), also known as methanethiol. [7]

Methanol is mainly produced in digesters. The formation of methanol is dependent on temperature, alkalinity, type of wood and pulping time. Alkali-catalyzed elimination of methanol from 4-O-methylglucuronic acid residues in hemicellulose and demethylation (removal of methyl group(s)) of lignin are assumed to be the primary mechanisms for methanol formation. [8] According to the experiments conducted by Zhu et al. [8] on pine (softwood), about 40 % of methanol forms from hemicellulose

and around 35 % from demethylation. The remaining methanol is the naturally present methanol in wood which releases instantly at the beginning of the pulp process. They also mentioned that demethylation of lignin did not contribute to the formation of methanol below the pulping temperature of 160 °C.

Around 43 % more methanol was produced in hardwood cooking (12.1 kg/oven dry tonne (ODT) pulp) compared to softwood cooking (8.5 kg/ODT pulp) when producing bleachable grade pulp. Additionally, soda pulping produced more methanol than kraft pulping due to the lower delignification rate and the higher amount of active alkali. [8]

The term turpentine is generally used for the volatile fraction separated from pine resin [9]. Crude sulphate turpentine is one of the main impurities in the kraft process. The amount of produced turpentine depends highly on the wood species with the average yield being 5 to 10 kg/t of pulp for pine species and slightly lower for spruces. It can be recovered from the digester relief condensates. [10]

The methoxyl groups of dissolved lignin and the hydrosulphide ions in the cooking liquor react to produce TRS with MM being the main compound formed during the cooking process. Ionized MM then reacts with the methoxyl groups to form DMS. While DMDS does not form directly during cooking, it can be produced when the black liquor gets in contact with air, and MM oxidizes. H₂S forms in stock washing and black liquor evaporation and storage. It is also produced in lime kilns when residual sodium sulphide decomposes. Additionally, H₂S is formed in the lower part of the recovery boiler but most of it normally oxidizes to sulphur dioxide in the upper part. [11]

2.1.2 Methanol segregation and liquefaction

After releasing from the wood during cooking in the digester, methanol transfers to the weak black liquor (WBL) and to the flash vapour from the blow tank. The vapour is then condensed into foul (digester) condensate. Methanol in the WBL evaporates in the evaporators and condenses into evaporator condensate. [12]

Steam stripping is used for the removal of volatile compounds from foul condensate. A steam stripper for removing methanol and other volatiles is shown in Figure 2. Since methanol increases the biochemical oxygen demand for waste water treatment, steam stripping has become an important part of pulp mills from an environmental point of view. [6] Furthermore, the removed pollutants can be burned and used as substitutes for fossil fuels in the mills [13].

The stripper off gas (SOG) is commonly liquified with a partial condenser. The liquified methanol can be used as a replacement for natural gas or oil in plant start-ups, for example. SOG can also be incinerated as a gas in the lime kiln or the recovery boiler. [12] An example of a liquid methanol system is presented in Figure 3. The obtained crude methanol contains typically at least 65 wt-% and up to 80 wt-% methanol [12, 14]. The incineration of crude methanol causes nitrogen and sulphur oxide emissions due to its ammonia and TRS content. Additionally, the handling of crude methanol is difficult because of its unpleasant odour. To supply the increasing demand of green methanol, processes have been developed to further purify crude methanol to commercial grade methanol [12], which is discussed in the following

section.

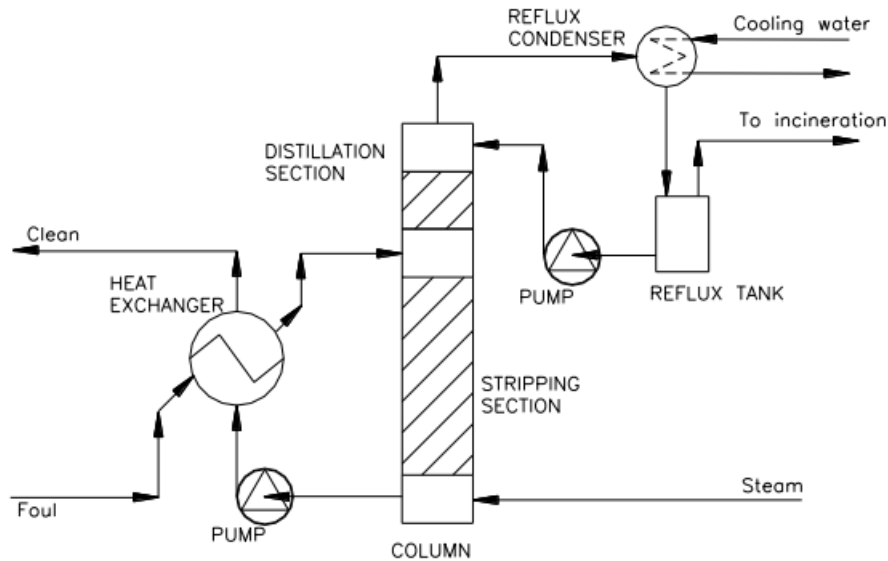


Figure 2: Steam stripper used for separation of volatiles from foul condensate [13].

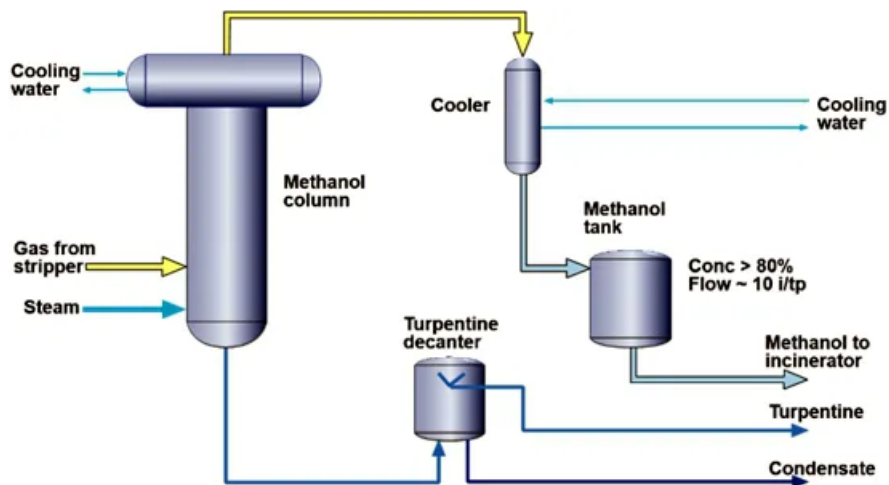


Figure 3: Typical system for methanol liquefaction [12].

2.1.3 Impurities in crude methanol

More than 150 compounds have been identified from crude methanol obtained from foul condensate stripping [15]. The main impurities are grouped in Table 1 with example compounds.

Table 1: The main components in crude methanol [15–17].

Component group	Example compounds	Characteristics
Alcohols	MeOH, EtOH	<ul style="list-style-type: none"> hydroxyl group polar
Ketones	Acetone	<ul style="list-style-type: none"> carbonyl group polar
Terpenes	α -pinene, β -pinene, α -terpineol	<ul style="list-style-type: none"> structure: $(C_5H_8)_n$, $n \geq 2$ highly non-polar and insoluble in water α-pinene hydrates to α-terpineol in the presence of H_2SO_4
Sulphurous compounds	4-mercapto-4-methyl-2-pentanone, (methylthio)alkanethiols, long-chain sulphides, TRS	<ul style="list-style-type: none"> odorous, flammable and toxic H_2S and MM ionize in aqueous solutions
Nitrogen compounds	Ammonia, amines, pyrrole	<ul style="list-style-type: none"> NH_3 highly soluble in methanol

It was determined by Niemelä [15] that the primary nitrogen component, ammonia, accounted for 85–95 % of the total nitrogen concentration (10–20 g/l). In addition to the above components, one common impurity in kraft mill condensates is guaiacol. It is a phenol which is found in concentration ranges between 20 and 80 mg/kg. [18]

Niemelä [15] also found that hardwood methanols only contained relatively small amounts of terpenes. The oil fraction of eucalyptus, however, can contain up to 90 % of cineole (eucalyptol), which is a monoterpene [19]. In softwoods, monoterpenes make up most of the turpentine [20]. Common monoterpenes are classified in Table 2.

Table 2: Monoterpenes found in softwood species [20, 21].

Structure	Example compounds	Amount in monoterpene fraction (m-%)	Average (m-%)
Acyclic	Myrcene	0–22	4
Monocyclic	Terpinenes	0–5	0.5
	Terpineols	0–67 (of total oil content)	-
	Limonene	1–83	13
	p-Cymene	<1	0.1
Bicyclic	Pinenes	12–96	60
	3-carene	0–64	10
	Camphene	0–35	3

As can be seen from Table 2, the amount of each monoterpene varies largely depending on the species. The composition also depends on the location of the species and, thus, different populations of the same species can have varying compositions [20]. An example of a crude methanol stream composition from softwood pulping is shown in Table 3.

Table 3: An example of the composition of a crude methanol stream from softwood pulping.

Component	Mass-%
Methanol	80
Water	10
TRS	2
Nitrogen compounds	1
Turpentine	5
Other (acetone, ethanol)	2

2.1.4 Crude methanol purification

As discussed previously, crude methanol obtained from foul condensates contains impurities that need to be removed in order to produce commercial-grade methanol. Some specifications for purified methanol published by International Methanol Producers & Consumers Association (IMPCA) are presented in Table 4.

Table 4: IMPCA specifications for commercial-grade methanol.

Specification	Limit	Unit
Purity on dry basis	≥ 99.85	m-%
Acetone	≤ 30	mg/kg
Ethanol	≤ 50	mg/kg
Water	≤ 0.1	m-%
Sulphur	≤ 0.5	mg/kg

In addition to the crude methanol purification process of ANDRITZ [14], similar systems have been developed by other companies, including Valmet [22], A.H. Lundberg Systems [23] and FPinnovations [24]. The flowsheets of the processes are shown in Figures 4–7.

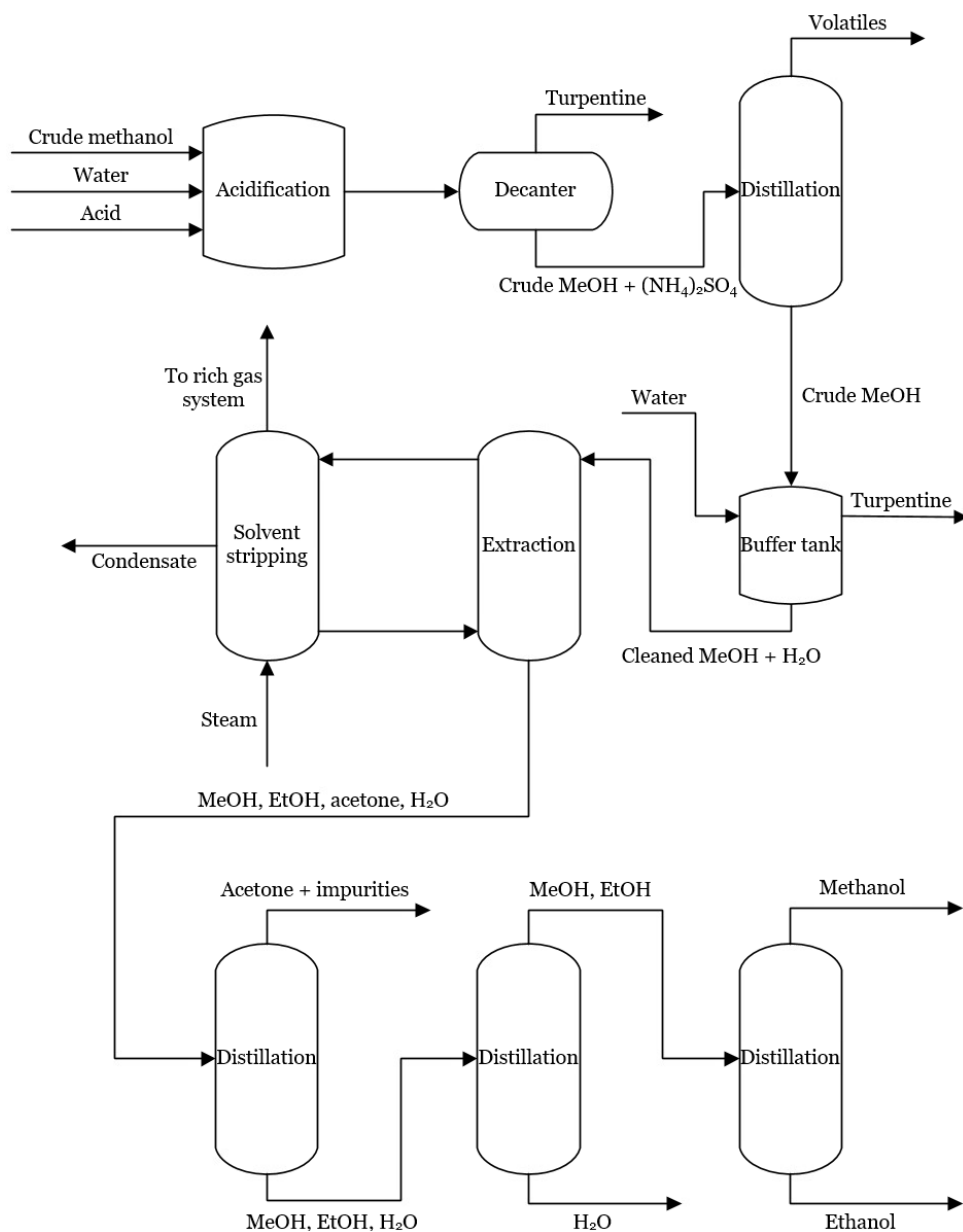


Figure 4: Crude methanol purification process of ANDRITZ. Adapted from the patent [14].

The process of ANDRITZ starts with adding acid, such as sulphuric acid, to convert the ammonia in the crude methanol into ammonium sulphate. The acidification also decreases the solubility of volatile TRS compounds, such as H₂S and MM. Turpentine is separated in a decanter. The solution is then distilled to remove the remaining volatile sulphurous compounds and separate methanol from the acid and non-precipitated ammonium salts. The distillation can be done in two separate columns or in a partition column. Water can be added to the cleaned methanol to facilitate phase separation and to increase the removal of heavier sulphur compounds and turpentine in the extraction column. A non-polar solvent, such as a mineral or paraffinic oil, is used for extraction

and it is regenerated in a stripping column. Finally, the solution is distilled in three steps to remove acetone, water, ethanol and other remaining impurities. [14]

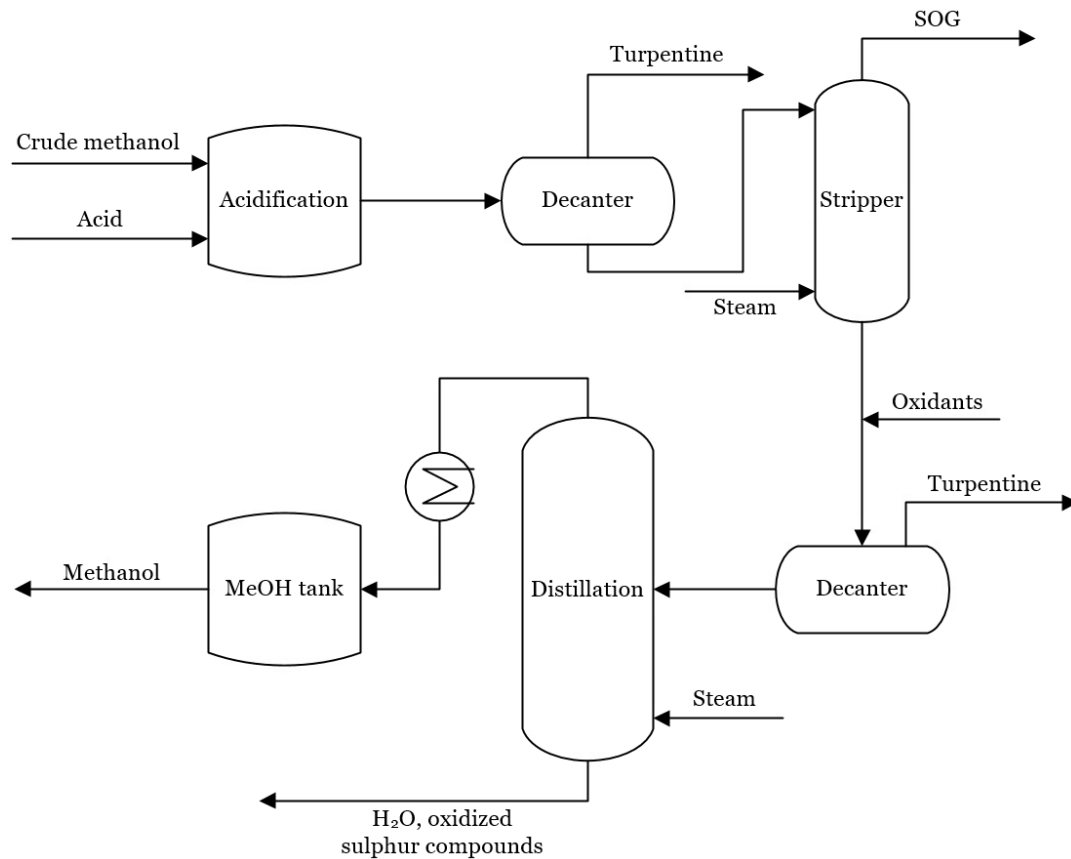


Figure 5: Crude methanol purification process of Valmet. Adapted from the patent [22].

Similar to the process of ANDRITZ, the Valmet process begins with acidifying the crude methanol. Another unit may also be added to add hydrocarbons, such as turpentine, if the hydrocarbon content is too low for a satisfactory extraction. A stripper is then used to remove pollutants. An oxidation agent can be added to the methanol containing condensate to oxidize sulphurous compounds and make them less volatile and, this, prevent them from transferring to the distillate. Finally, the distillate is condensed, and the final product can be collected from the methanol tank. [22]

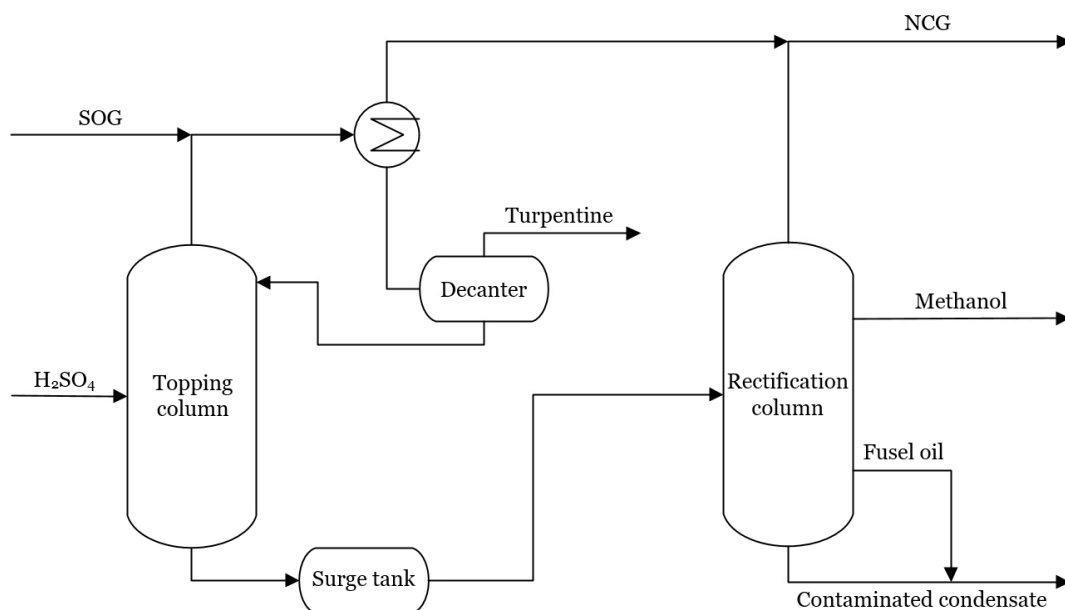


Figure 6: Crude methanol purification process of A.H. Lundberg Systems. Adapted from the patent [25].

The process designed by A.H. Lundberg starts with the decanting of turpentine and consists of two distillation columns. Unlike in the previous processes, sulphuric acid is added straight to the first column. The acid is fed to the mid-point of the column to prevent ammonium sulphate from forming and to ensure that ammonia evaporates at the top of the column before reacting with the acid. The pH is lowered to between 5 and 6 to release the dissociated H₂S and MM and allow them to rise through the column to the distillate. The methanol-rich bottom product goes to the surge tank from which it is pumped to the rectification column. In this column, methanol is separated from less volatile compounds, such as water and fusel oil (ethanol and ketones). The final product is collected slightly below the top of the packing. [23, 25]

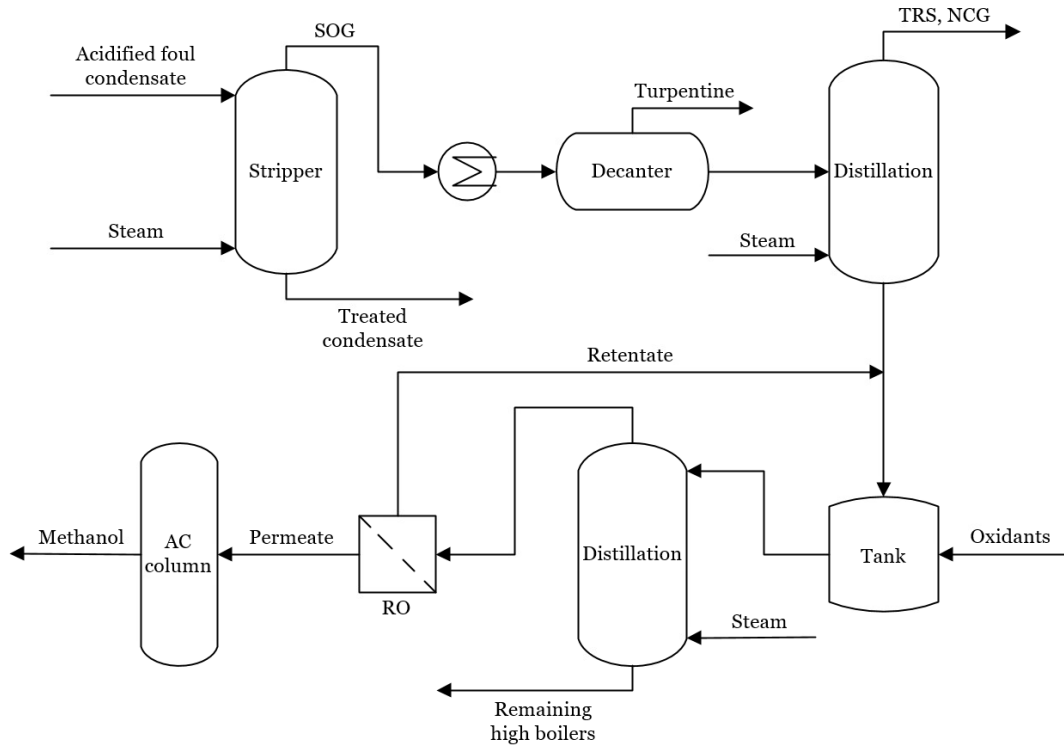


Figure 7: Crude methanol purification process of FPinnovations. Adapted from the patent [24].

The process of FPinnovations starts with stripping the acidified foul condensate. The condensed SOG is decanted into turpentine and methanol rich streams. The methanol rich stream is distilled twice to remove impurities. Oxidants or precipitation agents can be added to the methanol stream from the first column to enhance the removal of sulphur compounds. In contrast to the previous processes, the final purification is done with reverse osmosis and activated carbon. [24]

2.2 Thermodynamic models for phase equilibrium modelling

In addition to mass and energy balances, thermodynamics are a crucial part of modelling since information on vapour-liquid equilibrium (VLE) and liquid-liquid equilibrium (LLE) is needed for modelling distillation and extraction systems. [26, 27] Therefore, it is important to choose a correct thermodynamic model to get the most accurate simulation.

Several thermodynamic models have been developed for phase-equilibrium calculations in multicomponent systems. The activity coefficient models or excess Gibbs energy (G^E) models of Wilson, non-random two-liquid (NRTL [28]) and universal quasichemical (UNIQUAC [29]) are the most used due to their applicability to non-ideal solutions [30]. They are suitable choices for systems containing polar components at pressures below 10 atm and away from the critical region [27] which starts at the critical point where phase boundaries vanish. Above the critical temperature, a gas

cannot liquefy. Critical pressure is the pressure required to liquefy a gas at its critical temperature. [31] Since, NRTL and UNIQUAC can be used to describe liquid-liquid equilibrium (LLE), they are also suitable for extraction systems. In general, these models can be expressed as a function of temperature (T), composition (x) and set of BIPs (p):

$$\gamma_i = f(T, x, p) \quad (1)$$

where γ_i is the activity coefficient of species i . The drawback for these models is that they require experimental equilibrium data for fitting the BIPs. [32]

G^E models are used for the liquid phase interactions, and the vapour phase can be assumed to be ideal, or an equation of state (EOS), such as Redlich-Kwong, may be used. When the vapour phase is described by the ideal gas law, modified Raoult's law is used to calculate the vapour phase composition with Equation 2:

$$x_i \gamma_i P_{i,sat} = y_i P \quad (2)$$

where P is the overall pressure of the system and $P_{i,sat}$ is the saturation pressure of the component [33]. EOSs, on the other hand, calculate vapour pressures as a function of temperature, molar volume (V_m) and attraction (a) and volume (b) parameters:

$$p_{vap} = f(T, V_m, a, b) \quad (3)$$

EOSs can also be used for modelling both the liquid and vapour phase. They are generally suitable for non-polar components in the critical region [27]. Therefore, EOSs are commonly used for hydrocarbon mixtures in the petroleum industry, for example [32].

The original NRTL model has three adjustable parameters per binary pair. The third parameter, called the non-randomness parameter (α_{ij}), is recommended to be set between 0.2 and 0.5 depending on the nature of the mixture. [28] Up to ten parameters can be used on Aspen Plus and nine on CHEMCAD [34, 35]. The NRTL model defined in CHEMCAD and Aspen is presented below in Equation 4. The equation is used to calculate activity coefficients for species i in a mixture of n species.

$$\ln(\gamma_i) = \frac{\sum_{j=1}^n x_j \tau_{ji} G_{ji}}{\sum_{k=1}^n x_k G_{ki}} + \sum_{j=1}^n \frac{x_j G_{ij}}{\sum_{k=1}^n x_k G_{kj}} \left(\tau_{ij} - \frac{\sum_{m=1}^n x_m \tau_{mj} G_{mj}}{\sum_{k=1}^n x_k G_{kj}} \right) \quad (4)$$

where

$$G_{ij} = \exp(-\alpha_{ij} \tau_{ij}) \quad (5)$$

$$\tau_{ij} = A_{ij} + \frac{B_{ij}}{T} + C_{ij} \ln(T) + D_{ij} T \quad (\text{CHEMCAD}) \quad (6)$$

$$\tau_{ij} = a_{ij} + \frac{b_{ij}}{T} + e_{ij} \ln(T) + f_{ij} T \quad (\text{Aspen}) \quad (7)$$

Aspen has an additional adjustable parameter d_{ij} in the equation for α_{ij} :

$$\alpha_{ij} = c_{ij} + d_{ij}(T - 273.15 \text{ K}) \quad (8)$$

BIPs A_{ij} (a_{ij}), B_{ij} (b_{ij}), C_{ij} (e_{ij}) and D_{ij} (f_{ij}) are unsymmetrical which means that A_{ij} can not be equal to A_{ji} and so on. It is mentioned in the help section of CHEMCAD that the equation may be used with three (B_{ij} , B_{ji} and α_{ij}), five (B_{ij} , B_{ji} , A_{ij} , A_{ji} and α_{ij}), seven (B_{ij} , B_{ji} , A_{ij} , A_{ji} , C_{ij} , C_{ji} and α_{ij}) or nine (B_{ij} , B_{ji} , A_{ij} , A_{ji} , C_{ij} , C_{ji} , D_{ij} , D_{ji} and α_{ij}) parameters.

UNIQUAC has two adjustable parameters for each component pair. In addition, two pure component structural parameters, r and q , are required. [29] Aspen and CHEMCAD again have the option to use more parameters as they allow up to nine and eight parameters respectively [34, 35]. The UNIQUAC model is presented below in Equation 9.

$$\begin{aligned} \ln(\gamma_i) = & \ln\left(\frac{\phi_i}{x_i}\right) + \frac{z}{2}q_i \ln\left(\frac{\theta_i}{\phi_i}\right) + l_i - \frac{\phi_i}{x_i} \sum_{j=1}^n x_j l_j \\ & - q_i \ln\left(\sum_{j=1}^n \theta_j \tau_{ji}\right) + q_i - q_i \sum_{j=1}^n \left(\frac{\theta_j \tau_{ji}}{\sum_{k=1}^n (\theta_k \tau_{ki})}\right) \end{aligned} \quad (9)$$

where

$$\phi_i = \frac{x_i r_i}{\sum_{j=1}^n r_j} \quad (10)$$

$$\theta_i = \frac{x_i q_i}{\sum_{j=1}^n q_j} \quad (11)$$

$$\tau_{ij} = \exp\left(A_{ij} - \frac{U_{ij} - U_{jj}}{RT} + C_{ij} \ln(T) + D_{ij} T\right) \quad (12)$$

$$l_i = \frac{z}{2}(r_i - q_i) - r_i + 1 \quad (13)$$

$$z = 10 \quad (14)$$

In general, the optimization of the BIPs is more reliable with VLE data compared to LLE data. Since G^E models are highly non-linear, the algorithm used for the optimization problem may produce multiple parameter sets with similar values for the objective function. Additionally, LLE is more sensitive to the initial guesses used for BIPs which can cause inconsistencies. [36]

Group contribution methods, such as UNIQUAC functional-group activity coefficients (UNIFAC) [37], can also be used for distillation and extraction applications

[38]. Unlike the aforementioned models, UNIFAC only requires experimental data for the calculation of interaction parameters between functional groups, which can then be used for different mixtures [37]. UNIFAC has some weaknesses which are discussed in more detail in section 2.4.2.

Henry's law can be used to describe solubility of gases in dilute solutions at low pressures. It states that the amount of dissolved gas in a liquid is directly proportional to its partial pressure above the liquid. [39] It can be chosen which components follow Henry's law on Aspen Plus and CHEMCAD [34, 35]. Henry's law is used to represent the behaviour of dissolved gases or other supercritical components in activity coefficient models. [34] The most common thermodynamic models are collected in Figure 8 which proposes a process for choosing the most suitable model.

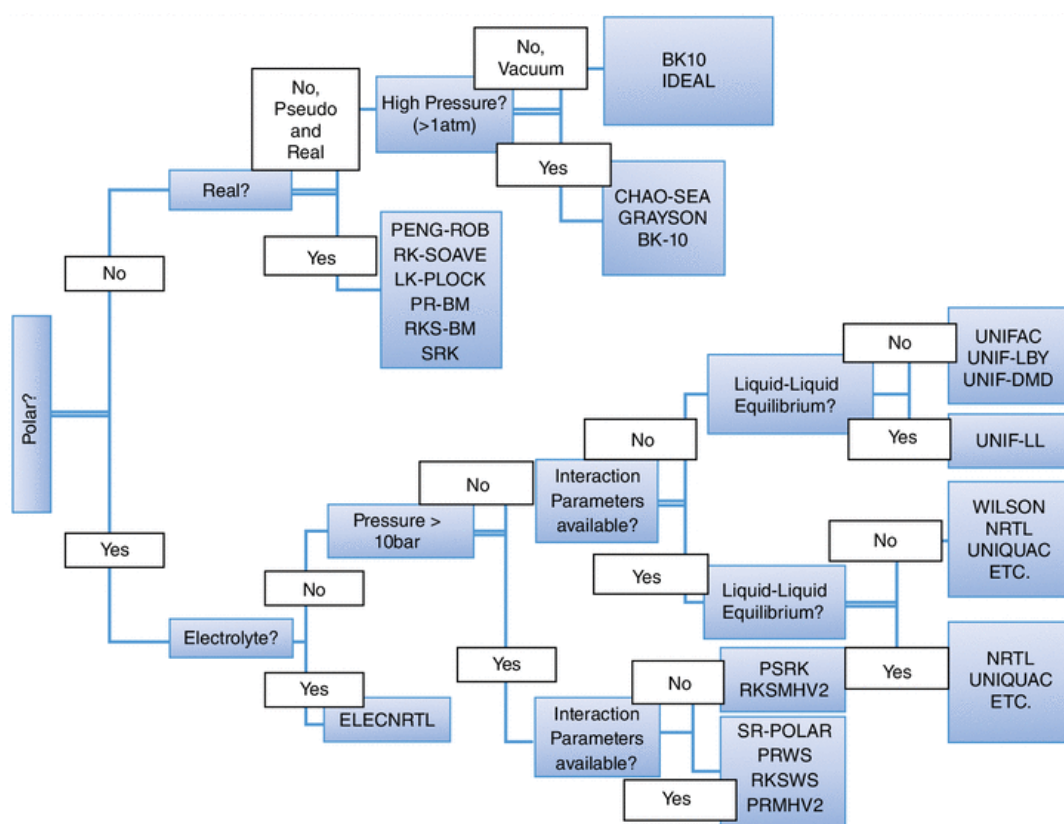


Figure 8: Model selection tree based on different properties of a mixture [27].

2.3 Steady-state simulation in CHEMCAD and Aspen Plus

Process simulation seeks to predict the real behaviour of a defined process under specified operating conditions. Several commercial simulation programs have been developed since the 1960s and they offer various modules for simulating unit operations. [40] In line with the scope of this work, steady-state simulation of distillation and liquid-liquid extraction with CHEMCAD and Aspen Plus are discussed in this section.

Most simulation programs, including CHEMCAD and Aspen Plus, have a built-in library for the thermodynamic models discussed previously. The default NRTL and

UNIQUAC models in Aspen use ideal gas law to model the vapour phase. The ideal gas assumption is usually valid for lower pressures, and the CHEMCAD user guide recommends using an EOS for the vapour phase when pressure exceeds 3 atm. [35]

Other available NRTL and UNIQUAC models in Aspen use Redlich-Kwong, Hayden-O'Connell (HOC) or Nothnagel EOSs for the vapour phase. [34] As for CHEMCAD, HOC or Marek and Standart can be chosen for the vapour phase. HOC is especially useful for mixtures containing carboxylic acids since it takes their dimerization into account [41].

After the model has been chosen, the programs look for BIPs from different databases. The BIPs can be regressed using experimental data if more accurate values are required or no BIPs are found from the databases. [27, 35] On Aspen Plus, the user can access the National Institute of Standards and Technology (NIST) ThermoData Engine to look up VLE or LLE data which can then be imported to the simulation file. Consistency tests can also be conducted to find out the data quality. [27]

2.3.1 Simulation of distillation

Aspen and CHEMCAD offer different types of blocks for distillation with varying levels of complexity. The models can be divided into shortcut and rigorous models as shown in Table 5.

Table 5: Distillation models in Aspen Plus and CHEMCAD [42, 43].

	Aspen Plus	CHEMCAD
Shortcut	DSTWU, Distl, SCFrac	SHOR
Rigorous	RadFrac, MultiFrac	TOWR, TOWER PLUS, SCDS

Shortcut models are not accurate when there is significant non-ideality in the liquid phase. However, they can be used as a initial design for rigorous models since rigorous models may fail to converge with bad initial estimates. Rigorous models calculate mass and energy balances for each stage in the column. These models can be divided into equilibrium-stage and rate-based models. In equilibrium-stage models, VLE calculations are affected by stage efficiencies which can be set by the user. [42] For example, Aspen Plus and CHEMCAD use the Murphree stage efficiency equation [34] which describes how close the vapour and liquid phases are to equilibrium on a stage:

$$E_{i,j}^M = \frac{y_{i,j} - y_{i,j+1}}{K_{i,j}x_{i,j} - y_{i,j+1}} \quad (15)$$

where K is the vapour-liquid distribution ratio and, thus, $K_{i,j}x_{i,j}$ is the vapour mole fraction at equilibrium. Subscripts i and j refer to the component and stage indices respectively.

In rate-based models, the models solve mass and heat transfer equations. Even though rate-based models are more realistic, they are less used due to the difficulty of predicting interfacial area and mass transfer coefficients. [42] The rigorous models of Aspen Plus and CHEMCAD can also perform vapour-liquid-liquid equilibrium (VLLE) calculations with two liquid phases [34, 43].

A major part of simulation studies on methanol distillation focus on the purification of crude methanol obtained from synthesis gas. PRO/II and Aspen Plus are widely utilised for simulation with NRTL and Wilson being the most used thermodynamic models. [44]

2.3.2 Simulation of extraction

CHEMCAD and Aspen Plus have a multistage extraction block for rigorous simulation of extraction systems [34, 43]. They allow the user to specify the temperature and pressure profiles of the column. Additionally, stage efficiencies can be specified. In Aspen, the key components for the first and second liquid phases have to be specified to help the algorithm solve the composition profiles in the extraction column [34]. Both programs can also produce ternary diagrams which are helpful in finding operating regions for extraction processes. [34, 43]

2.4 Equilibrium data for crude methanol

2.4.1 Vapour-liquid and liquid-liquid equilibrium

Kuosa et al. [45] modelled VLE of kraft pulp mill condensates using UNIQUAC. The components chosen for the model were water, methanol, H₂S, MM, DMS, DMDS, oxygen and nitrogen. Terpenes were represented by α -pinene. It was also mentioned in their paper that other suitable compounds to be included could be carbon dioxide, acetone, methyl ethyl ketone, α -terpineol and guaiacol. [45] Methyl ethyl ketone was not found in crude methanol in the study of Niemelä [15] or mentioned by Olsson and Zacchi [18], so it was excluded from this work. Even though pinenes are the most common monoterpenes, as discussed in section 2.1.3, it could be beneficial to also include other common terpenes, such as limonene and 3-carene, in simulations to get the most accurate results.

The work by Olsson and Zacchi [18] gives an overview on the available VLE data on kraft mill condensates in addition to their own measurements. They also present BIPs for Wilson and NRTL models obtained from Aspen Plus data regression tool. VLE and LLE data found for different binary pairs from their article and other literature is presented in Table 6. When multiple VLE measurements were found for a pair, both isobaric and isothermal datasets were chosen. Additionally, consistency tests were run on Aspen Plus if VLE data was available on the NIST database to find the most reliable data. Furthermore, it should be noted that most data points for H₂S–water/DMS/MM, MM–water and DMS–water systems were measured in higher pressures than atmospheric pressure and they might not be useful for BIP regression for the process discussed in this work.

Table 6: Binary VLE and LLE (*) data found from the literature.

	H ₂ S	MM	DMS	DMDS	MeOH	EtOH	Acetone	Water	α -pin.	α -terp.
Guaiacol					[46]	[47]	[46]	[18], [47]*		
α -terpineol				[18]		[48]		[18]		
α -pinene					[18], [49]*	[50]		[18], [49]*		
Water	[51], [52]*	[53–55]	[56]	[18], [57]*	[58, 59]	[60, 61]	[62, 63]			
Acetone					[64, 65]	[66, 67]				
EtOH			[68]	[69, 70]	[71, 72]					
MeOH	[73]	[74, 75]	[76]	[69, 70]						
DMDS		[77]								
DMS	[78]									
MM	[79]									

As can be seen from Table 6, phase equilibrium data on systems containing guaiacol, α -terpineol or α -pinene is scarce in the literature. Only a couple of VLE experiments have been done for terpenes in general in addition to α -pinene. In the review article of Puentes et al. [80], BIPs for the NRTL model were regressed for linalool and linalool oxide in ethanol and water. Binary LLE data was found for methanol + limonene/ β -pinene systems [81, 82]. Additionally, some studies have been conducted regarding LLE of ternary systems containing terpenes. LLE data was found for the following ternary systems:

- water + methanol + α -pinene/ β -pinene/limonene [49]
- methanol + ethanol + α -pinene [82]
- water + acetone + α -pinene/ β -pinene/limonene [83]

When liquid phase splitting occurs, it is recommended to also include VLLE data in the parameter optimization if possible [84]. However, VLLE data was only found for H₂S + water systems [85, 86]. As mentioned by Marcilla et al. [87], most used G^E models, such as NRTL and UNIQUAC, often fail to describe VLE and VLLE of binary systems with liquid-liquid splitting with adequate accuracy. Therefore, it is common to use different sets of BIPs for VL, LL and VLL regions [88]. To address the problem, Marcilla et al. [88] proposed a modified NRTL model which improved results for ternary systems with these regions by introducing an additional term for the Gibbs energy term.

2.4.2 Prediction of lacking experimental data

As mentioned in the previous section, experimental data is lacking for multiple component pairs in crude methanol. Therefore, it might be useful to use models that predict equilibria without the need for experiments. These kind of models are discussed next. It should be noted, however, that BIPs for components with very low concentrations (in the ppm range) can be left out since they have no effect on the results. BIPs with water should be determined for every compound since large non-idealities occur with water and organic compounds. [89]

UNIFAC, published in 1975, predicts the VLE behaviour of a system by calculating activity coefficients from group interaction parameters between functional groups

[37]. The published parameters can be obtained from the Dortmund Data Bank. Aspen Plus and CHEMCAD also have a feature that uses UNIFAC to estimate missing BIPs in G^E models [34, 35].

UNIFAC has certain flaws, such as inaccurate results for excess enthalpies and activity coefficients at infinite dilution. Thus, the modified UNIFAC (Dortmund) method, which uses temperature dependent group interaction parameters, was released in 1987. More main groups were defined and an empirically adjusted combinatorial part was included to enhance the results for asymmetric systems. [90] The improvement can be seen in Figure 9 where the UNIFAC models are compared to UNIQUAC. The modified model still has some weaknesses, such as unreliable results when molecules have a lot of functional groups. Moreover, systems that deviate little from Raoult's law cause challenges in the estimation when vapour pressure differences are small. [89]

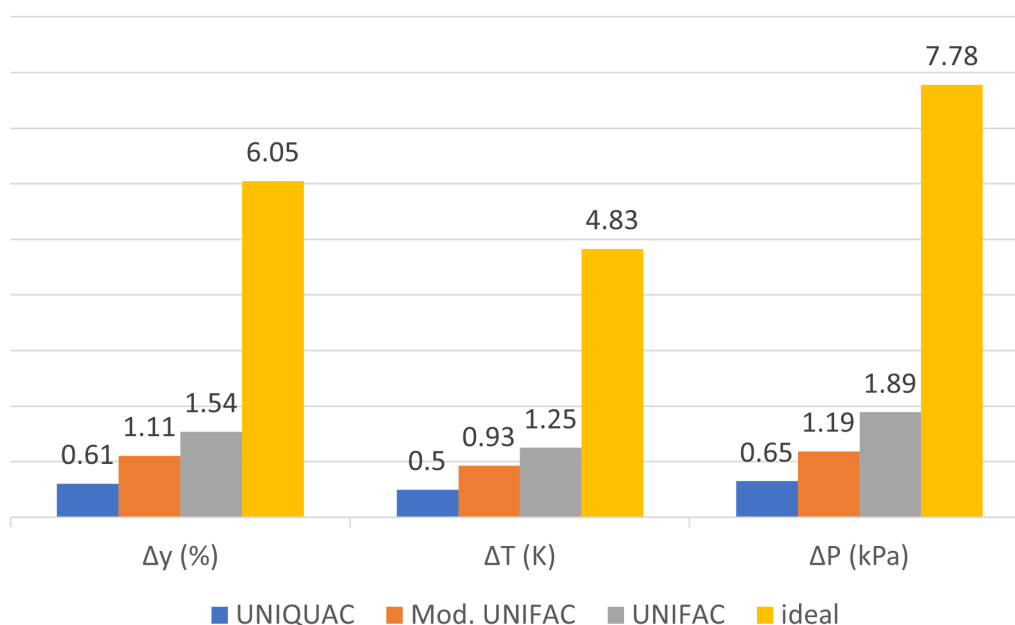


Figure 9: Deviations in vapour mole fraction (y), temperature (T) and pressure (P) between different models compared to experimental data. Adapted from [91].

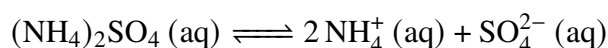
A method called conductor-like model for real solvents (COSMO-RS), which predicts fluid phase thermodynamics of mixtures, was released in 1995 [92]. Unlike group contribution methods, such as UNIFAC, it does not describe interaction between molecular surfaces with group parameters but with local surface descriptors. The conductor screening charge density, which describes the molecular surface polarity, is the most important descriptor. It can be calculated for each molecule separately with quantum chemical programs like COSMO. [93] The free energy of a compound in the ideal gas can be estimated using COSMO-RS but Klamt et al. [94] recommend to use experimental vapour pressures for pure compounds in VLE calculations.

In recent years, the use of artificial intelligence has been researched as a tool for predicting VLE to avoid the time-consuming VLE experiments. Felton et al. [95]

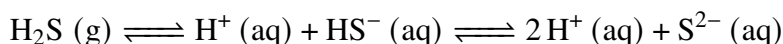
developed a deep learning model for predicting activity coefficients from molecular structures using directed message passing neural networks. Their model was considerably faster than COSMO-RS. Sun et al. [96] predicted VLE behaviour with machine learning (ML) by training their model with available VLE data using artificial neural network and random forest approaches. Their vision for the future would be that the user could input the boiling points and critical temperatures of compounds to calculate VLE properties for binary mixtures. Winter et al. [97] developed a model called SPT-NRTL which uses ML to predict NRTL parameters and uses them to calculate activity coefficients.

2.5 Electrolyte models

Ammonium sulphate in the acidified crude methanol dissolves in water:



Ammonium sulphate is a strong electrolyte since it dissociates completely in aqueous solutions. [98] Therefore, it is relevant to discuss thermodynamic models that can be used for electrolytes. In addition, hydrogen sulphide and methyl mercaptan dissolve and ionize in water solutions [45]:



However, these electrolytes are weaker compared to ammonium sulphate due to their lower dissociation in water [45]. It can be seen from the reaction equations that lowering the pH and, thus, increasing the concentration of hydrogen ions lowers the ionization of hydrogen sulphide and methyl mercaptan in accordance with Le Chatelier's principle.

Electrolyte models are constructed as a sum of long range and short range interactions:

$$\ln(\gamma_i) = \ln(\gamma_{i,tr}) + \ln(\gamma_{i,sr}) \quad (16)$$

The short range interactions can be modelled with e-NRTL, e-UNIQUAC, e-UNIFAC and Pitzer models. All of the mentioned models use the Debye-Hückel theory for the long range Coulomb interactions. [99] CHEMCAD and Aspen have e-NRTL and Pitzer models in their model libraries.

The electrolyte NRTL is the default model for electrolyte solutions in Aspen Plus since it is the most versatile of the built-in models. It is combined with Redlich-Kwong EOS to calculate vapour phase fugacities in VLE systems. [27] e-NRTL is also available in CHEMCAD [35]. The advantage of e-NRTL is that it simplifies to the traditional NRTL model when no electrolytes are present. Therefore, the same BIPs for molecule-molecule interactions can be used for both models. When electrolytes are present, interaction parameters for molecule-electrolyte and electrolyte-electrolyte pairs are required. [100]

The Pitzer model has three adjustable BIPs. Ternary parameters are also included in the complete model but they are often neglected in practice. [100] e-NRTL would seem to be the more convenient choice compared to Pitzer since the interactions between molecules can be modelled with the same BIPs that are used in the original NRTL model. Especially in the case of systems with many components, such as crude methanol, a lot of work would be required to obtain the BIPs for the Pitzer model from experimental data. It is mentioned by Gmehling et al. [100], however, that e-NRTL produces significant errors for systems with two or more electrolytes or a solvent mixture, and the results in these cases should be used as a qualitative estimation.

3 Simulation of the methanol purification process

The simulation of the purification process of ANDRITZ is discussed in this section. As mentioned in the patent, the first distillation step in Figure 4 can be split into two separate columns [14]. These columns are referred to as the sulphur and methanol columns in the following sections. The part of the process that was simulated with CHEMCAD NXT 1.1.1 and Aspen Plus V12.1 is presented in Figure 10.

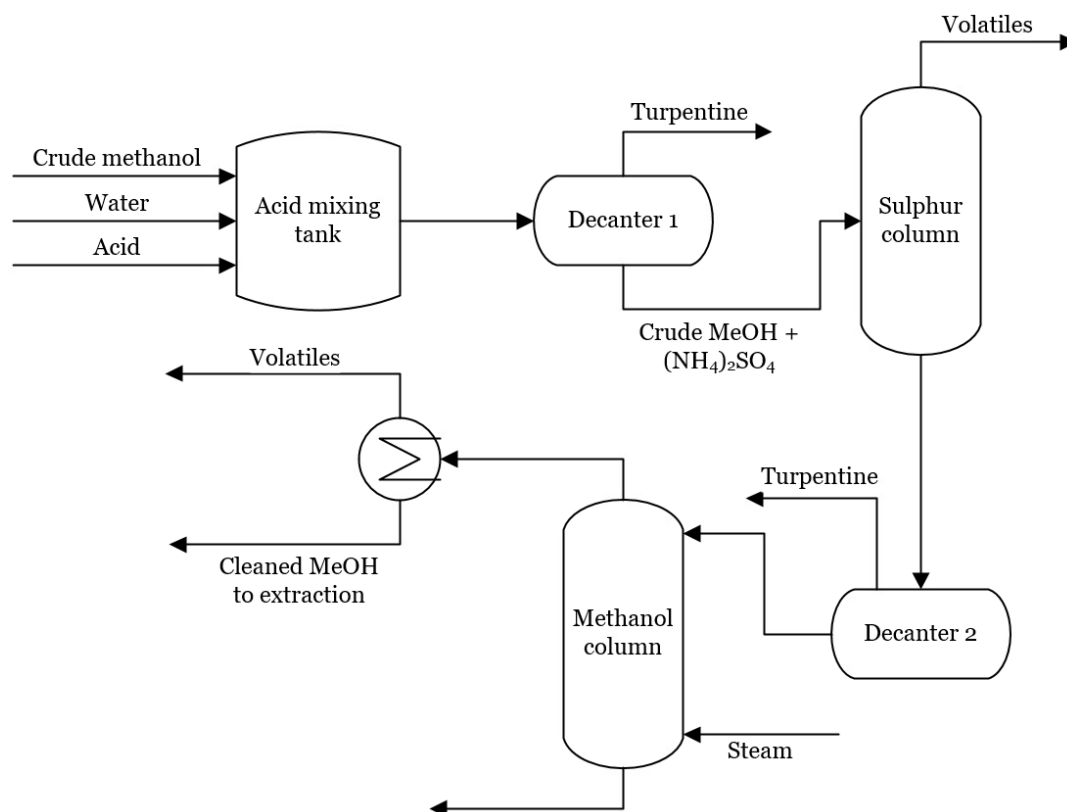


Figure 10: Flowsheet of the simulated process.

3.1 Selection of required compounds in methanol purification

The components selected for the simulation part were water, methanol, ethanol, acetone, ammonia, MM, DMS, DMDS, H₂S, α - and β -pinene, 3-carene, limonene, α -terpineol and guaiacol. 3-Carene was not found from the CHEMCAD database, so it was created manually by defining its UNIFAC groups and using UNIFAC to estimate its physical properties. Table 7 shows which BIPs were found for NRTL and UNIQUAC from the CHEMCAD and APV121 VLE-IG databanks. The BIPs found only from Aspen were copied to CHEMCAD. If no BIPs were found for a pair, the pair was assumed to be ideal and the BIPs were 0.

Table 7: BIPs for NRTL and UNIQUAC found from Aspen Plus (A) and CHEMCAD (CC) databanks.

	H ₂ O	MeOH	EtOH	Ace.	NH ₃	MM	DMS	DMDS	H ₂ S	α -pin.	β -pin.	3-car.	Lim.	α -terp.
Gua.		A		A										
α -terp.														
Lim.										A				
3-car.														
β -pin.										A				
α -pin.														
H ₂ S														
DMDS														
DMS		A+CC				A+CC								
MM		A+CC		A										
NH ₃	A													
Ace.	A+CC	A+CC	A+CC											
EtOH	A+CC	A+CC												
MeOH	A+CC													

3.2 Prediction of lacking equilibrium data

The standard version of UNIFAC was chosen to model the decanters since it yielded rather accurate results for terpene–water–methanol systems. A ternary LLE diagram for the system α -pinene–water–methanol is shown in Figure 11.

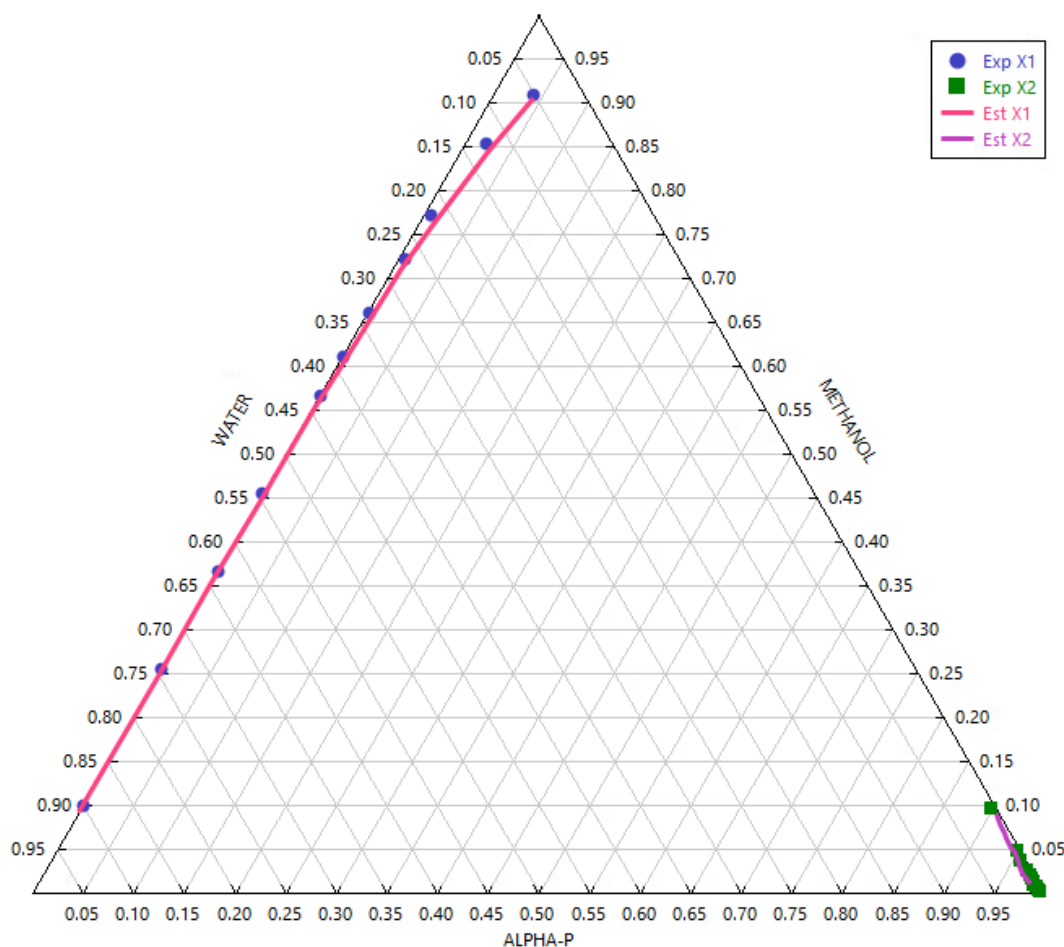


Figure 11: Ternary LLE diagram of the system α -pinene–water–methanol calculated with UNIFAC compared to experimental data by Tamura and Li [49] at 25 °C.

The UNIFAC groups of 3-carene were not found from Aspen or CHEMCAD databases so the groups were set manually on both programs. The molecular structure of 3-carene and its UNIFAC groups are shown in Figure 12 and Table 8 respectively.

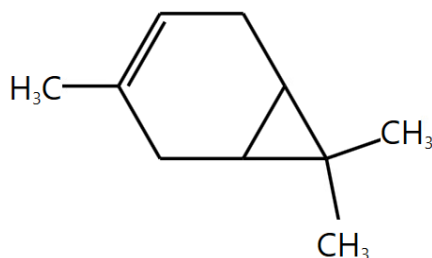


Figure 12: Molecular structure of 3-carene.

Table 8: UNIFAC groups chosen to represent 3-carene.

Group number in Aspen	Description	No. of occurrences
1000	>C<	1
1005	>CH-	3
1010	>CH ₂	2
1015	-CH ₃	2
1160	Aromatic C-CH ₃	1

3.3 Setting up the simulations

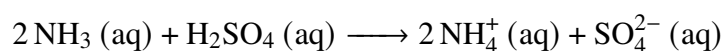
NRTL was chosen as the thermodynamic model due to its suitability for the highly polar solution of the process. CHEMCAD and Aspen used the default BIPs found from their respective databases. The simulation flowsheets are shown in Appendix A. The inlet stream composition of crude methanol shown in Table 9 was based on data from kraft pulp mills and laboratory analyses.

Table 9: Composition of the crude methanol stream.

Component	Flow (g/s)	Mass-%
Water	57.1	5.7
Methanol	754.0	75.4
Ethanol	36.0	3.6
Acetone	4.9	0.5
Ammonia	36.5	3.7
MM	30.0	3.0
DMS	16.4	1.6
DMDS	0.9	0.1
α -pinene	30.5	3.1
β -pinene	9.3	0.9
3-carene	21.9	2.2
Limonene	2.4	0.2
Total	1000	100

3.3.1 Acid mixing tank

The acid mixing tank was modelled with stoichiometric reactor blocks REAC and RStoic on CHEMCAD and Aspen Plus respectively. The reactor was set as isothermal and the temperature (55 °C) was obtained from plant data. The following reaction was defined in the reactor by setting the stoichiometric coefficients of the reactants:



The acid flow rate was controlled with a feed-forward controller to feed a stoichiometric amount of acid to react with the ammonia in the crude methanol. A

feed-backward controller was used to control the flow of dilution water into the mixing tank to prevent the ammonium sulphate from precipitating. The specification was that the mass fractions of NH_4^+ and SO_4^{2-} summed to 0.06. CONT blocks were used on CHEMCAD to define the controllers. On Aspen, a calculator block was used as the feed-forward controller, and a design specification was defined to correspond to a feed-backward controller.

3.3.2 Decanters

Flash blocks FLAS (CHEMCAD) and Flash3 (Aspen) were used to model the two decanters. As discussed previously, UNIFAC was used as the thermodynamic model.

3.3.3 Columns

SCDS and RadFrac blocks were used on CHEMCAD and Aspen respectively to model the columns. The column specifications are presented in Table 10. The temperature of the sulphur column condenser was specified with a design specification that varied the reflux ratio to achieve a temperature of 45 °C in the condenser. No reboiler was defined for the methanol column, and a flash block was used to represent a condenser. The liquid feed and the steam flow into the methanol column were set onto the top and bottom stages respectively.

Table 10: Specifications of the columns.

	Sulphur column	Methanol column
Column type	Trayed	Trayed
Top pressure (kPa)	97.3	93.3
Condenser temperature (°C)	45	63.5
Condenser pressure drop (kPa)	2	2
Column pressure drop (kPa)	15	15

4 Simulation results

4.1 Comparison of CHEMCAD and Aspen Plus simulations

The simulations were first run with the default BIPs found from the databases without any regressed parameters. The results of each unit operation are compared in the following.

4.1.1 Acid mixing tank

The ammonia converted into ammonium sulphate in the mixing tank with a trace amount of ammonia left in the outlet stream. The flow rate of the dilution water controlled with the feed-backward controller was 1.25 kg/s in both simulations.

4.1.2 The first decanter

The Aspen Plus simulation could not converge when NH_4^+ and SO_4^{2-} ions were present in the first decanter due to the missing UNIFAC groups of the ions. Since the ions could not be expressed with UNIFAC, it was assumed that the ions would go to the methanol-rich phase. This was done with a separator block placed upstream of the decanter which separated the ions from the decanter feed and fed them to the sulphur column with the methanol-rich stream.

The CHEMCAD simulation did not run into any problems and it was able to handle the ions in the decanter without any UNIFAC parameters. In the CHEMCAD simulation, 99.5 m-% of the ions went to the methanol-rich phase, so the assumption made in the Aspen simulation caused only a small difference in the results of the first decanter. Phase separation was predicted very similarly in both programs as shown in Table 11. The separation efficiency was calculated as follows:

$$\frac{m_{i,turpentine}}{m_{i,feed}} \cdot 100 \% \quad (17)$$

where $m_{i,turpentine}$ and $m_{i,feed}$ were the mass flows of component i in the turpentine-rich phase and the feed stream into the decanter respectively. In total, turpentine made up 96.0 and 96.9 m-% of the total turpentine-rich phase in CHEMCAD and Aspen respectively.

Table 11: Turpentine separation into the turpentine-rich phase in the first decanter.

Component	Feed flow (g/s)	Separation (m-%)	
		CC	Aspen
α -pinene	30.5	93.6	94.4
β -pinene	9.3	93.5	94.3
3-carene	21.9	97.2	96.0
Limonene	2.4	92.6	93.6
Total	18.8	94.8	94.9

4.1.3 Sulphur column

The mass balances of the sulphur column are presented in Table 12. The separation efficiencies of TRS compounds into the distillate were 81.9 and 81.5 m-% from the column feed for the CHEMCAD and Aspen simulations respectively.

Table 12: Mass balances of the sulphur column on CHEMCAD (CC) and Aspen.

Component	Inlet (g/s)		Bottoms (g/s)		Distillate (g/s)	
	CC	Aspen	CC	Aspen	CC	Aspen
Water	1311.5	1311.6	1311.3	1311.4	0.18	0.15
Methanol	753.5	753.5	736.2	736.6	17.2	16.9
Ethanol	36.0	36.0	35.9	35.8	0.09	0.15
Acetone	4.87	4.87	1.04	0.71	3.83	4.15
Ammonia	0.005	0.006	0	0	0.005	0.006
NH ₄ ⁺	38.5	38.7	38.5	38.7	0	0
SO ₄ ²⁻	102.4	102.9	102.4	102.9	0	0
MM	29.7	29.7	0.28	0.30	29.5	29.4
DMS	15.5	15.4	7.19	7.36	8.30	8.09
DMDS	0.88	0.87	0.88	0.87	0	0
α -pinene	1.96	1.68	1.96	1.68	0	0
β -pinene	0.61	0.52	0.61	0.52	0	0
3-carene	0.61	0.87	0.61	0.87	0	0
Limonene	0.18	0.16	0.18	0.16	0	0
Total	2296.1	2296.7	2237.0	2237.9	59.1	58.9

While the flow rates were almost identical, differences were observed in the reflux ratios and condenser duties. The reflux rate was higher in CHEMCAD (384 g/s) compared to Aspen (362 g/s) which caused higher values for the reflux ratio and condenser duty.

The temperature of the bottom product, reflux ratio (RR) and condenser duty of the sulphur column from the simulations are presented in Table 13. In addition, the temperature profiles are plotted in Figure 13.

Table 13: Temperature of the bottom product, reflux ratio (RR) and condenser duty of the sulphur column.

	Bottoms T (°C)	RR (mol/mol)	Condenser duty (kW)
CHEMCAD	83.7	8.3	-411.5
Aspen	84.1	7.8	-386.5

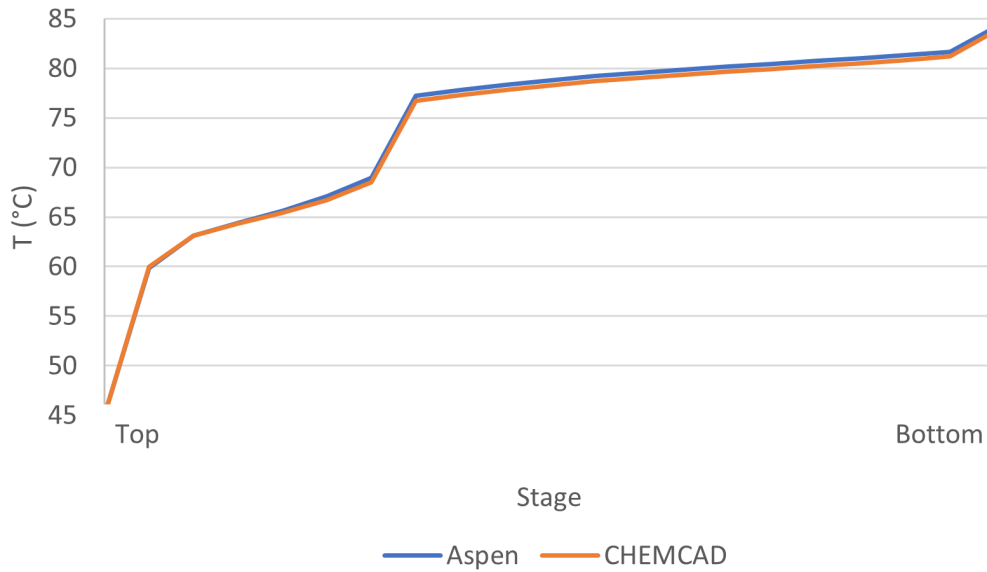


Figure 13: Temperature profiles of the sulphur column on CHEMCAD and Aspen.

4.1.4 The second decanter

The efficient separation of turpentine in the first decanter caused the turpentine concentration to be very low (0.1 m-%) in the feed to the second decanter. Therefore, no phase separation occurred in either simulation.

4.1.5 Methanol column

The mass balances of the methanol column are presented in Table 14. The LP steam flow in the feed is not included in the table.

Table 14: Mass balances of the methanol column on CHEMCAD and Aspen.

Component	Inlet (g/s)		Bottoms (g/s)		Distillate (g/s)	
	CC	Aspen	CC	Aspen	CC	Aspen
Water	1311.3	1311.4	1609.4	1610.0	202.2	201.78
Methanol	736.2	736.6	149.6	170.3	586.6	566.2
Ethanol	35.9	35.8	8.87	5.9	27.02	29.93
Acetone	1.04	0.71	0	0	1.04	0.71
Ammonia	0	0	0	0	0	0
NH ₄ ⁺	38.5	38.7	38.5	38.7	0	0
SO ₄ ²⁻	102.4	102.9	102.4	102.9	0	0
MM	0.28	0.3	0	0	0.28	0.3
DMS	7.19	7.4	0.06	0.06	7.14	7.30
DMDS	0.88	0.87	0.78	0.78	0.09	0.09
α -pinene	1.96	1.68	1.92	1.64	0.05	0.04
β -pinene	0.61	0.52	0.60	0.51	0.01	0.01
3-carene	0.61	0.87	0.60	0.86	0.01	0.01
Limonene	0.18	0.16	0.18	0.15	0.002	0.002
Total	2237.0	2237.9	1912.9	1931.8	824.5	806.4

No significant differences were observed in the results. The heat duties of the condenser and the bottom product temperatures are presented in Table 15. The temperature profiles were almost identical as was the case in the sulphur column. The profiles are shown in Figure 14.

Table 15: Temperature of the bottom product and condenser duty of the methanol column.

	Bottoms T (°C)	Condenser duty (kW)
CHEMCAD	95.4	-1170
Aspen	94.6	-1163

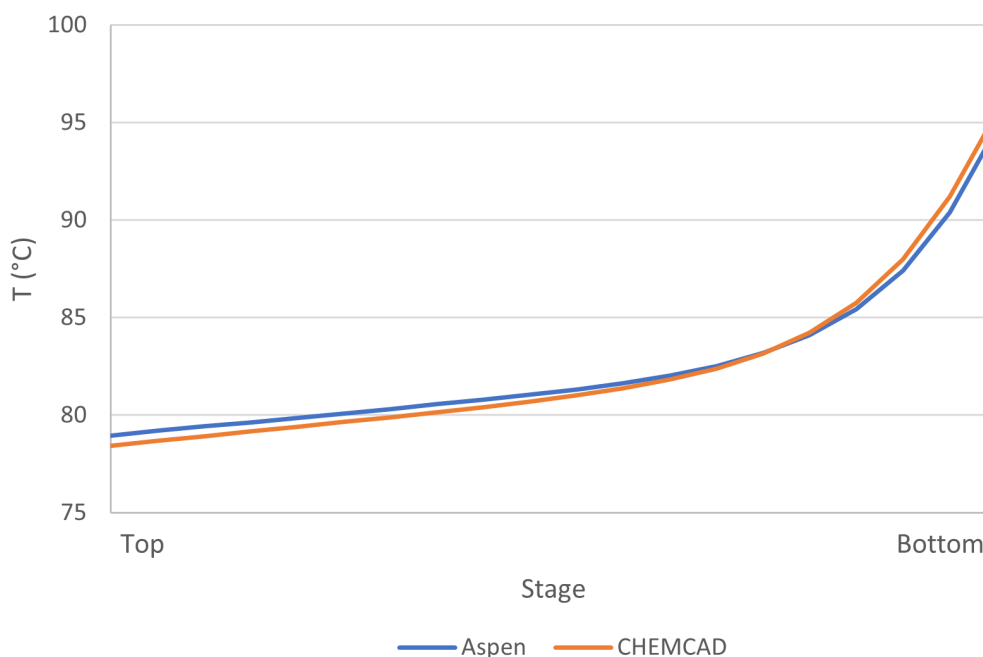


Figure 14: Temperature profiles of the methanol column on CHEMCAD and Aspen.

79.7 and 76.9 % of methanol was separated into the distillate on CHEMCAD and Aspen respectively. The respective methanol yields for the whole process were 77.8 and 75.2 %. The lower yield from Aspen can be explained with the lower amount of methanol in the distillate of the methanol column which was probably caused by the difference between BIPs in the CHEMCAD and Aspen databases. Figure 15 shows that CHEMCAD produced a bubble point curve with slightly lower temperatures for the methanol–water component pair which might explain the higher volatility of methanol in CHEMCAD compared to Aspen.

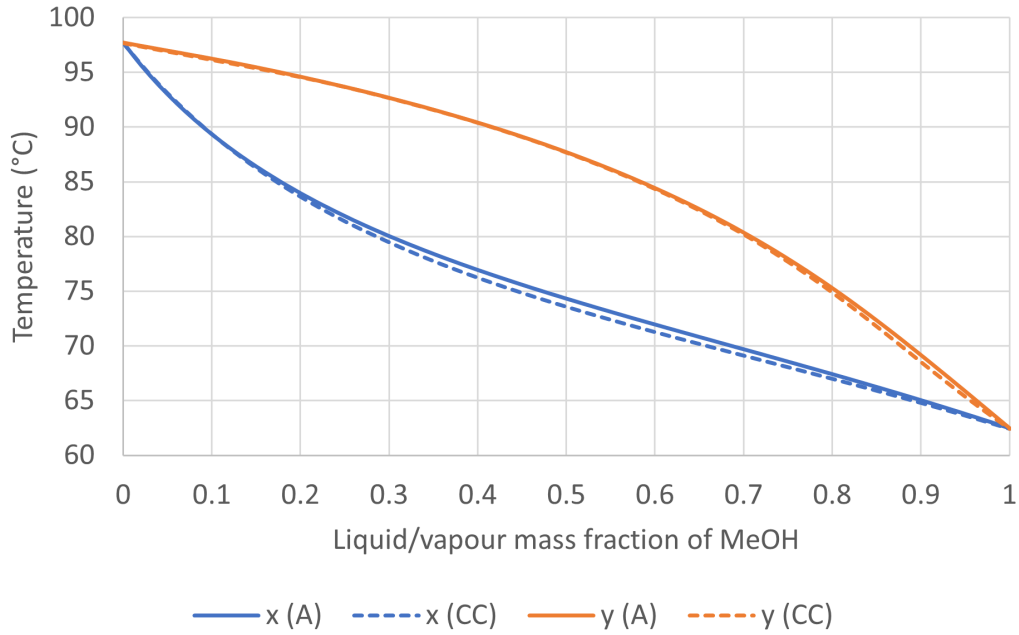


Figure 15: Comparison of Txy diagrams of methanol–water in CHEMCAD and Aspen.

4.2 Effects of regressed binary interaction parameters

After the simulations were run with the database BIPs, missing parameters were added to study their effect on the results. Several BIPs were copied from the study of Olsson and Zacchi [18] due to the lack of availability of equilibrium data, and some were regressed on Aspen and CHEMCAD from experimental VLE and LLE data. The BIPs for water–DMDS were obtained from the NISTV121 NIST-RK database from Aspen. BIPs were only regressed from data in the relevant temperature and pressure range at around 40 to 100 °C and 1 atm. The missing BIPs for water–terpene and methanol–3-carene systems were estimated with UNIFAC. The updated BIP matrix after the additions is shown in Table 16, and the regressed BIPs with root mean square percentage errors (RMSPE) are reported in Table 17. RMSPE is a common method for measuring forecast accuracy. It is defined as

$$RMSPE = \sqrt{\frac{1}{n} \sum_{i=1}^n \left(\frac{Y_i - \hat{Y}_i}{Y_i} \right)^2} \quad (18)$$

where n is the number of data points, Y_i is the measured value and \hat{Y}_i is the value estimated by the model. [101] The phase equilibrium diagrams from the regressions compared to experimental data are presented in Appendix B.

Table 16: BIPs used for the second simulations. Regressed BIPs are marked with R followed by the data source, and UF marks BIPs estimated with UNIFAC.

	H ₂ O	MeOH	EtOH	Ace.	NH ₃	MM	DMS	DMDS	H ₂ S	α -pin.	β -pin.	3-car.	Lim.	α -terp.
Gua.	[18]	A		A										
α -terp.	[18]	[18]												
Lim.	UF	R [81]								A				
3-car.	UF	UF												
β -pin.	UF	R [82]								A				
α -pin.	[18]	[18]												
H ₂ S	[18]	[18]				[18]								
DMDS	A	R [69]	R [69]			[18]								
DMS	[18]	A+CC				A+CC								
MM	[18]	A+CC		A										
NH ₃	A													
Ace.	A+CC	A+CC	A+CC											
EtOH	A+CC	A+CC												
MeOH	A+CC													

Table 17: Regressed BIPs with root mean square percentage errors.

Comp. <i>i</i>	Comp. <i>j</i>	a_{ij}	a_{ji}	b_{ij}	b_{ji}	α_{ij}	RMSPE (%)
MeOH	DMDS	0	0	431.6	507.5	0.48	0.39
MeOH	Limonene	1.36	-6.46	220.7	2226.3	0.30	0.73
MeOH	β -pinene	0.52	-5.16	452.2	1875.3	0.30	0.85
EtOH	DMDS	0	0	338.7	396.3	0.50	0.31

Parameters b_{ij} , b_{ji} and α_{ij} were regressed for the MeOH/EtOH–DMDS pairs. For the MeOH–limonene/ β -pinene pairs, α_{ij} was fixed at 0.3 and the a and b BIPs were regressed. Finally, the rest of the missing BIPs were estimated with UNIFAC and the simulations were run for the third time. However, the changes were minimal compared to the second simulation in both programs, and, thus, those results are not discussed any further.

4.2.1 Sulphur column

The mass balances of the sulphur column with regressed BIPs are shown in Table 18 below.

Table 18: Mass balances of the sulphur column on CHEMCAD and Aspen with regressed BIPs.

Component	Inlet (g/s)		Bottoms (g/s)		Distillate (g/s)	
	CC	Aspen	CC	Aspen	CC	Aspen
Water	1310.9	1311.6	1310.6	1311.4	0.30	0.21
Methanol	753.5	753.5	734.4	734.2	19.1	19.3
Ethanol	36.0	36.0	35.9	35.8	0.06	0.18
Acetone	4.87	4.87	1.26	0.66	3.61	4.21
Ammonia	0.01	0.01	0	0	0.01	0.01
NH ₄ ⁺	38.5	38.7	38.5	38.7	0	0
SO ₄ ²⁻	102.4	102.9	102.4	102.9	0	0
MM	29.7	29.7	0	0	29.7	29.7
DMS	15.5	15.4	0	0	15.5	15.4
DMDS	0.88	0.87	0.57	0.43	0.31	0.44
α -pinene	1.96	1.68	1.95	1.64	0.02	0.04
β -pinene	0.61	0.52	0.60	0.52	0.01	0
3-carene	0.61	0.87	0.27	0.87	0.33	0
Limonene	0.18	0.16	0.18	0.16	0	0
Total	2295.6	2296.7	2226.6	2227.2	69.0	69.5

The only significant differences in the flows were in the distillate rate and in the flows of sulphurous compounds. The distillate rate increased by around 10 g/s in both simulators. Therefore, the reflux ratios of the sulphur column decreased to 7.2 and 6.7 in CHEMCAD and Aspen respectively, which caused the condenser duties to decrease to -405.7 and -383.6 kW. This was caused mainly by the fact that all of DMS evaporated to the distillate, whereas in the first simulations, around 50 % of it remained in the bottom product. Furthermore, 35 and 51 % of DMDS evaporated into the distillate while in the first simulations it remained in the bottom product. Consequently, the separation efficiency of TRS compounds into the distillate increased to 98.8 and 99.1 % in CHEMCAD and Aspen respectively.

The Txy diagram of the water–DMS system for both cases are shown in Figure 16 where the effect of regressed BIPs is clearly seen. The updated BIPs for the DMS–water pair caused the boiling point of the binary system to be lower already at low concentrations of DMS. This was due to the high non-ideality and insolubility of the two compounds predicted by the model which then caused all of DMS to evaporate. Similar behaviour was also observed for water and DMDS which is shown in Figure 17. Azeotropes formed at water mass fractions of 0.02 and 0.19 and temperatures of 36.8 and 84.8 °C for DMS/DMDS–water systems respectively. The low temperatures of the bubble point curve of the DMS–water system explains the complete evaporation of DMS when the sulphur column condenser was operated at 45 °C. As for DMDS, it was observed that when BIPs for both DMDS–water and DMDS–methanol were used, DMDS partly evaporated into the sulphur column distillate. If BIPs were defined for only one of the pairs, practically no evaporation of DMDS occurred.

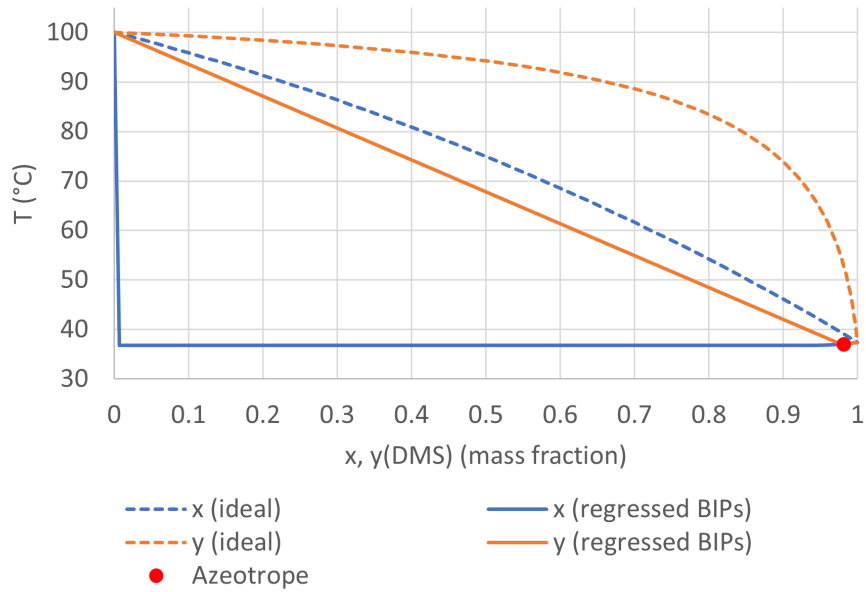


Figure 16: Txy diagrams for the system water–DMS with and without regressed BIPs from Olsson and Zacchi [18] for the NRTL model at 1 atm.

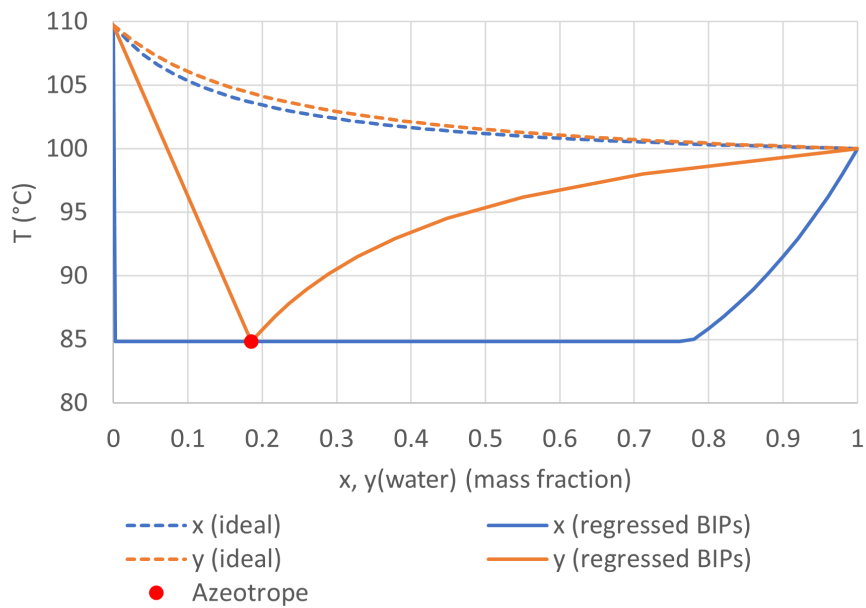


Figure 17: Txy diagrams for the system water–DMDS with and without the BIPs from the Aspen NISTV121 NIST-RK database for the NRTL model at 1 atm.

4.2.2 Methanol column

The mass balances of the methanol column with regressed BIPs are shown in Table 19 below.

Table 19: Mass balances of the methanol column on CHEMCAD and Aspen with regressed BIPs.

Component	Inlet (g/s)		Bottoms (g/s)		Distillate (g/s)	
	CC	Aspen	CC	Aspen	CC	Aspen
Water	1310.6	1311.4	1607.9	1608.7	203.1	203.0
Methanol	734.4	734.2	147.5	167.9	586.9	566.3
Ethanol	35.9	35.8	8.8	5.8	27.15	29.96
Acetone	1.26	0.66	0	0	1.26	0.66
Ammonia	0	0	0	0	0	0
NH ₄ ⁺	38.5	38.7	38.5	38.7	0	0
SO ₄ ²⁻	102.4	102.9	102.4	102.9	0	0
MM	0.0	0.0	0	0	0.0	0.0
DMS	0.0	0.0	0	0	0.0	0.0
DMDS	0.57	0.43	0	0	0.57	0.43
α -pinene	1.95	1.64	0.01	0.01	1.94	1.63
β -pinene	0.60	0.52	0	0.03	0.60	0
3-carene	0.27	0.87	0	0.21	0.27	0.66
Limonene	0.18	0.16	0	0.06	0	0
Total	2226.6	2227.2	1905.1	1924.4	821.9	803.1

Due to the increased separation efficiency of TRS compounds in the sulphur column, the TRS content of the distillate decreased from 9.1 and 9.5 to 0.7 and 0.5 g/kg in CHEMCAD and Aspen respectively with DMDS being the only TRS compound in the distillate. The DMDS content was higher with the updated BIPs compared to the initial simulations (0.1 g/kg) because of its increased volatility. Even though the top stage temperature was around 79 °C, which is lower than the temperature of the DMDS–water azeotrope, DMDS evaporated completely. If no BIPs were used for DMDS–water, DMDS stayed in the bottom product. The BIPs for DMDS–methanol did not affect the results.

The remaining terpenes evaporated into the distillate, while previously they were in the bottom product. Similarly to DMS and DMDS, terpenes formed minimum boiling heterogeneous azeotropes with water and methanol with the regressed BIPs which increased their volatility. The azeotropic compositions are presented in Table 20. The Txy diagram of α -pinene–water system is presented in Figure 18 as an example of terpene–water systems.

If regressed BIPs were used only for either terpene–water or terpene–methanol pairs, less evaporation occurred. For example, when BIPs for only α -pinene–water were used, 10 m-% of α -pinene evaporated. When the BIPs for α -pinene–methanol were added, over 99 m-% of the compound evaporated. Due to the increased evaporation of terpenes, the turpentine content of the methanol column distillate increased from 80.8 and 76.3 mg/kg to 3650 and 3580 mg/kg in CHEMCAD and Aspen respectively.

Table 20: Azeotropic compositions of terpene–water/MeOH systems predicted by NRTL at 1 atm.

System	Boiling point (°C)	m-% of terpene
α -pinene–water/MeOH	95.2 / 64.5	58.9 / 15.0
β -pinene–water/MeOH	96.5 / -	50.7 / -
3-carene–water/MeOH	97.1 / -	45.3 / -
Limonene–water/MeOH	97.6 / -	40.4 / -

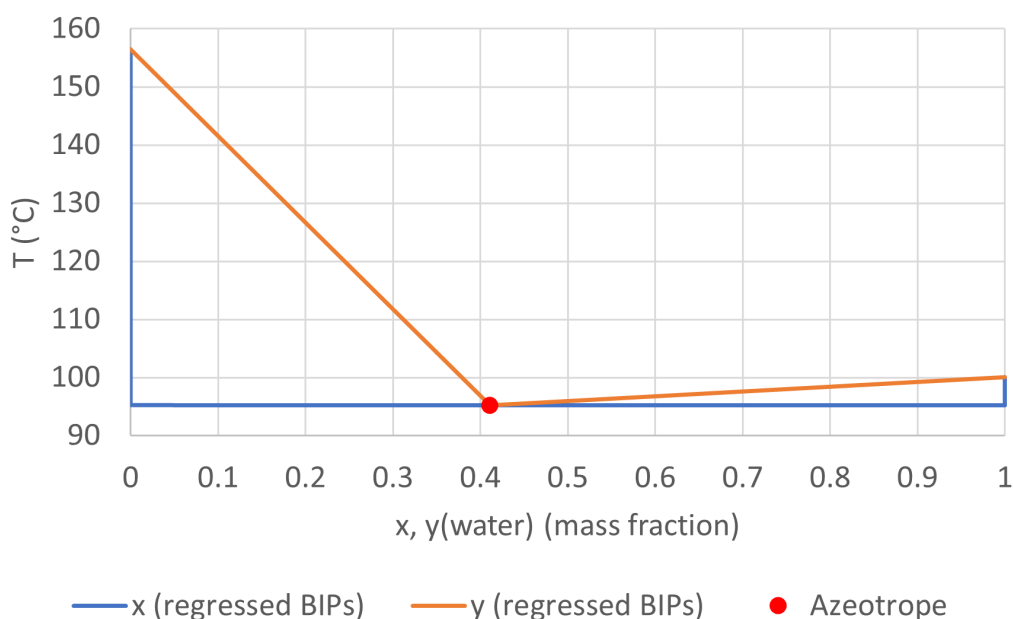


Figure 18: Txy diagram for the system α -pinene–water with regressed BIPs by Olsson and Zacchi [18] for the NRTL model at 1 atm.

There were no significant changes in the condenser duties or bottom product temperatures. The methanol separation efficiency increased slightly from 79.7 and 76.9 to 79.9 and 77.1 % in CHEMCAD and Aspen respectively. The methanol yield of the process remained the same in both simulations, however, since more methanol was lost into the sulphur column distillate.

4.3 Comparison of decantation simulation results to experimental data

The results from the simulated decanter on CHEMCAD were compared to a decantation test performed in a laboratory. The mass of the crude methanol sample was 300.2 g, and 390 g of dilution water was added. The composition of the feed is presented in Table 21. The dilution water flow was set at 390 g/s in the simulation.

Table 21: Composition of the feed into the decanter in the simulation.

Component	Flow (g/s)	Mass-%
Water	15.8	5.26
Methanol	243.7	81.2
Ethanol	10.0	3.33
Acetone	1.09	0.36
Ammonia	3.64	1.21
MM	0.42	0.14
DMS	5.00	1.66
DMDS	1.85	0.61
H ₂ S	0.05	0.02
α -pinene	8.69	2.89
β -pinene	2.60	0.87
3-carene	6.13	2.04
Limonene	1.22	0.41
Total	300.2	100

The results are presented in Table 22. The separation efficiencies were calculated in the same way as in section 4.1.2. Small amounts of α -terpinolene and camphene were found in the sample in the laboratory test. They were modelled with limonene and α -pinene as model compounds respectively in the simulation due to similar physical properties. Additionally, dimethyl trisulphide from the sample was assumed to be DMDS since it was not in the component database of CHEMCAD.

For comparison, the decanter was also simulated with NRTL as the thermodynamic model. The BIPs for the binary pairs water–methanol, water– α -pinene and methanol– α -pinene were first regressed from the experimental data by Tamura and Li [49] on CHEMCAD. The BIPs for terpene–TRS pairs were estimated with UNIFAC LLE since there were no database BIPs or experimental data available.

Table 22: Comparison of laboratory data to simulation results on TRS separation in a decanter.

Component	Separation to turpentine phase (m-%)		
	Laboratory	UNIFAC	NRTL
α -pinene	>99	96.6	92.7
β -pinene	>99	96.6	88.5
3-carene	>99	99.0	93.0
Limonene	>99	96.3	88.1
Terpenes in total	99.8	97.4	91.9
MM	61.1	0.8	3.5
DMS	56.6	7.3	27.1
DMDS	73.7	4.1	11.4
H ₂ S	100	0.5	1.5
TRS in total	61.5	6.1	21.6

The mass of the of the turpentine-rich phase was 8.4 m-% of the crude methanol sample in the laboratory test. The respective values for the UNIFAC and NRTL models were 6.2 and 6.3 m-%. While the separation of turpentine was predicted rather accurately, especially with UNIFAC, there was a large difference in the amount of sulphurous compounds separated into the turpentine-rich phase. NRTL was more accurate in predicting the solubility of TRS compounds into the turpentine-rich phase compared to UNIFAC. It is also possible that H₂S or other TRS compounds might have evaporated from the decanted sample which caused an error in the results. Finally, it should be noted that the separation of turpentine was almost 100 % in the laboratory test, which is unlikely in an continuously operated industrial-scale decanter. Thus, it would be useful to obtain data from a plant to get more realistic results.

5 Sensitivity analyses

The sensitivity analysis tools were used on CHEMCAD and Aspen Plus to study the effects of different compounds on the process outputs at varying concentrations. Additionally, the effects of varying the temperature of the sulphur column condenser and the steam flow into the methanol column were studied. The regressed BIPs from Table 16 were used. The pressures of the columns and the duty of the sulphur column condenser were kept constant in all of the following analyses.

The total flow rates of TRS compounds and turpentine were decreased by 75 to 25 % and increased by 25 to 100 % compared to the base case at 25 % intervals. Consequently, the total mass fraction of TRS and turpentine varied from 1.3 to 9.6 % and 1.7 to 12 % respectively in the feed stream. The distribution of the TRS and turpentine compounds were kept the same as in the previous simulations. The rest of the component flow rates were kept constant. Apart from increasing the flow of H₂S to 3 g/s, the same feed flow composition was used in the base case as in the previous simulations.

5.1 TRS compounds

The temperature of the sulphur column condenser was first fixed at 45 °C, and the effects of increasing TRS content in the feed stream were studied. Figure 19 shows that increasing the TRS concentration in the feed did not affect the overall yield of the process but it increased the amount of TRS in the methanol column distillate. The only TRS compound in the distillate was DMDS in all of the cases. While more methanol was lost into the sulphur column distillate at higher TRS concentrations, the volatility of methanol was higher also in the methanol column and, thus, the yield remained constant. More DMDS evaporated into the sulphur column distillate in Aspen and, thus, the TRS concentration of the methanol column distillate was lower in Aspen.

If the goal was to keep the TRS content constant in the bottoms, the sulphur column condenser would be required to operate at higher temperatures to counter the increased TRS concentration in the feed. However, as discussed further in section 5.4, higher condenser temperatures cause a decrease in methanol yield. If the methanol yield was also to be kept constant, an increase in the steam flow into the methanol column would be required. This would increase the amount of methanol in the distillate and balance out the loss of methanol in the sulphur column.

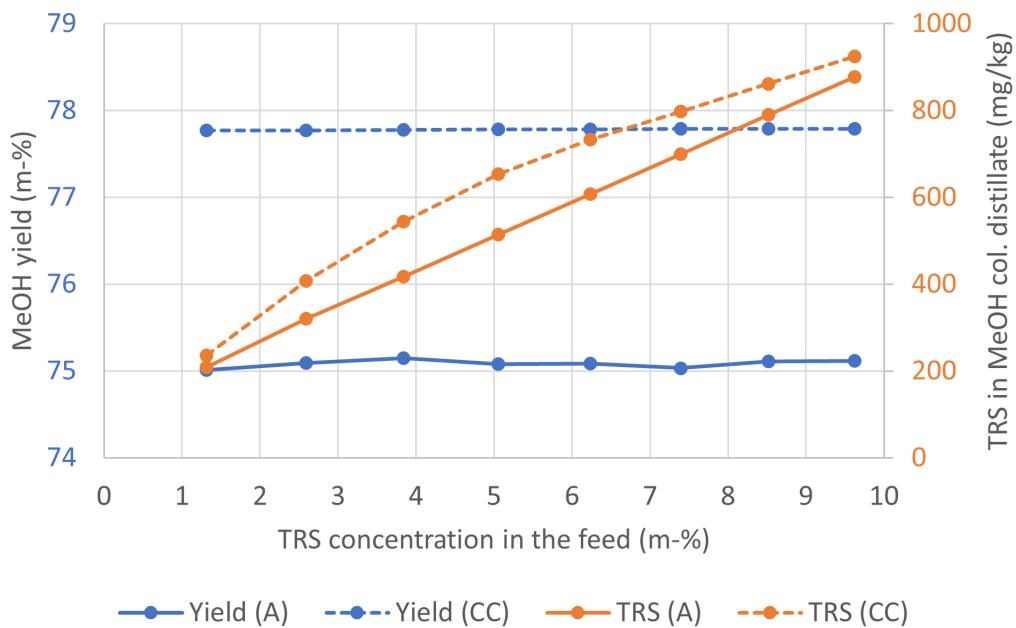


Figure 19: Sensitivity analysis on the effect of TRS concentration on the yield and TRS content in the methanol column distillate. (T of the sulphur column condenser = 45 °C)

When the TRS concentration was increased in the feed, the duty of the sulphur column condenser decreased due to the lower reflux rate. The condenser duty was found to be less sensitive to changes in TRS concentration in CHEMCAD compared to Aspen. As seen in Figure 20, the decrease in the cooling duty was much larger in Aspen due to the larger decrease in the reflux rate especially at TRS concentrations above 5 m-%.

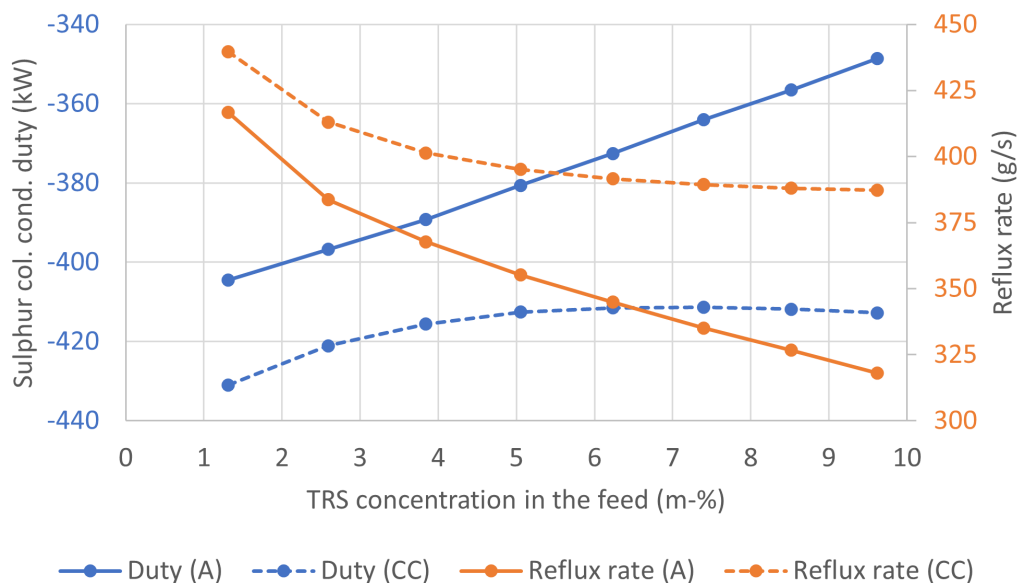


Figure 20: Sensitivity analysis on the effect of TRS concentration on the duty of the sulphur column condenser (T of the sulphur column condenser = 45 °C)

5.2 Turpentine

The separation efficiency of turpentine in the first decanter increased with increasing turpentine flow as seen in Figure 21. Therefore, there was only a 19 and 10 % relative difference in the turpentine content of the methanol product between the first and last case in CHEMCAD and Aspen respectively. No phase separation was observed in the second decanter in any of the cases.

The turpentine content of the methanol column distillate was slightly higher in CHEMCAD in most of the cases due to the more efficient separation of turpentine in the methanol column. Additionally, increasing the turpentine content increased the volatility of methanol in the methanol column while the methanol flow into the sulphur column distillate stayed constant. Therefore, the yield increased from 76.9 and 74.2 % in the first case to 79.0 and 76.3 % in the last case in CHEMCAD and Aspen respectively. Thus, the steam flow into the methanol column could be decreased slightly at higher turpentine concentrations to lower the operating cost, and the yield would still stay constant.

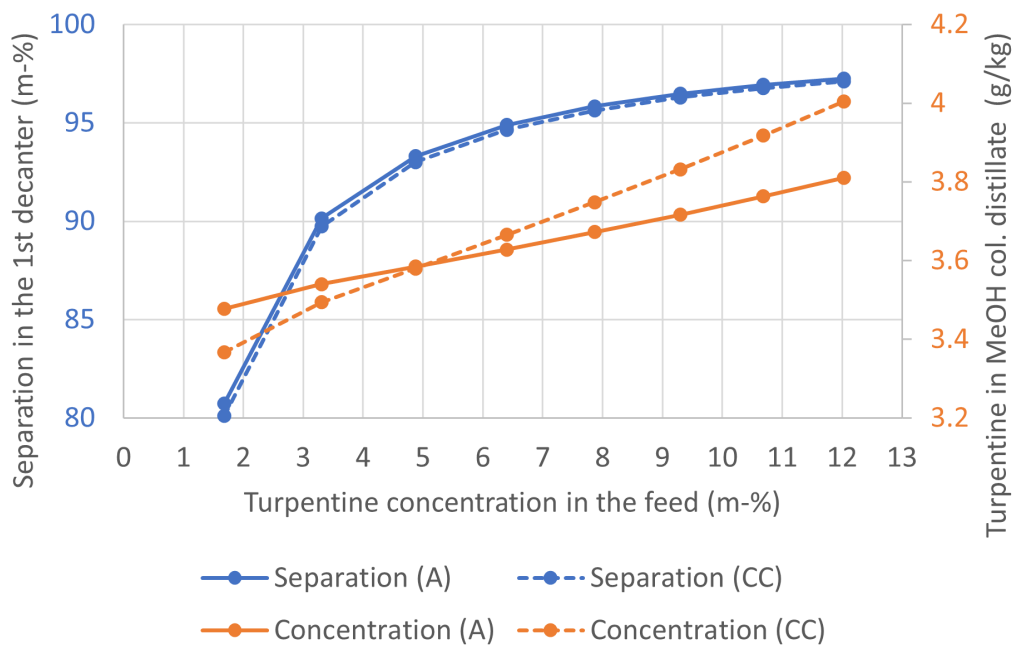


Figure 21: Sensitivity analysis on the effect turpentine concentration on the turpentine separation in the first decanter and turpentine content in the MeOH column distillate. (T of the sulphur column condenser = 45 °C)

The separation of TRS compounds into the turpentine-rich phase in the first decanter increased linearly with increasing turpentine content in the feed. Therefore, a small decrease was observed in the TRS concentration in the methanol column distillate as shown in Figure 22.

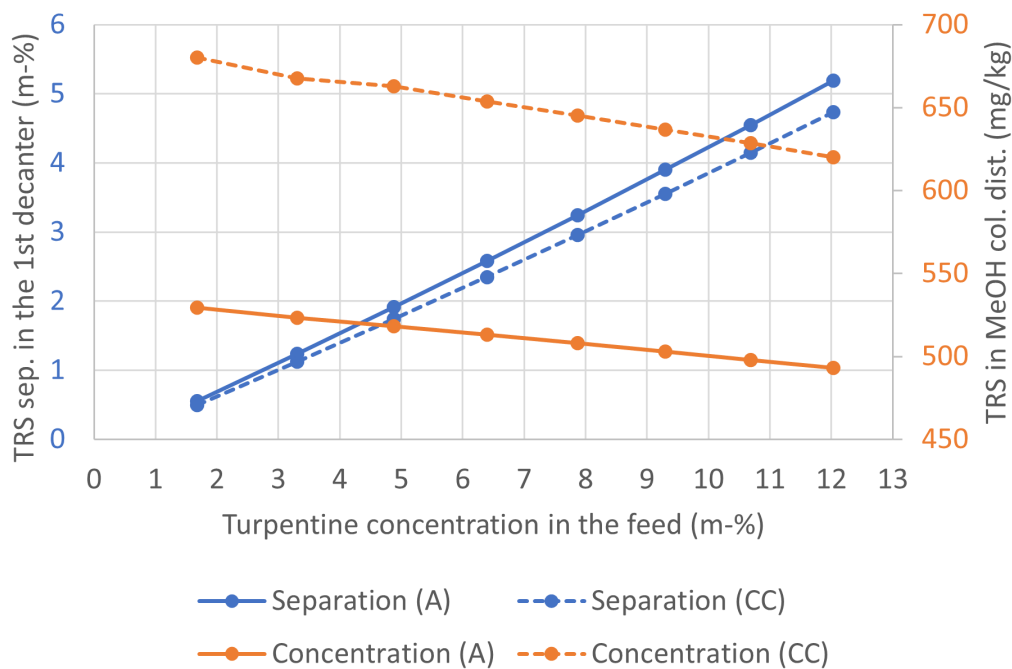


Figure 22: Sensitivity analysis on the effect of turpentine concentration on TRS separation in decantation and TRS concentration in the MeOH column distillate. (Temperature of the sulphur column condenser = 45 °C)

5.3 Alpha-terpineol and guaiacol

The feed flow rates of α -terpineol and guaiacol were varied from 0 to 10 g/s at 2 g/s intervals which corresponded to 0 to 3.3 in mass percentages. The separation of α -terpineol into the turpentine-rich phase increased in the first decanter with higher feed concentrations. The separation efficiency was much lower compared to terpenes, however. Similar to terpenes (Fig. 22), higher concentration of α -terpineol increased the solubility of TRS compounds into the turpentine-rich phase as seen in Figure 23. Over 99 m-% of the remaining α -terpineol in the methanol–water phase was obtained from the bottom product of the methanol column in all of the cases.

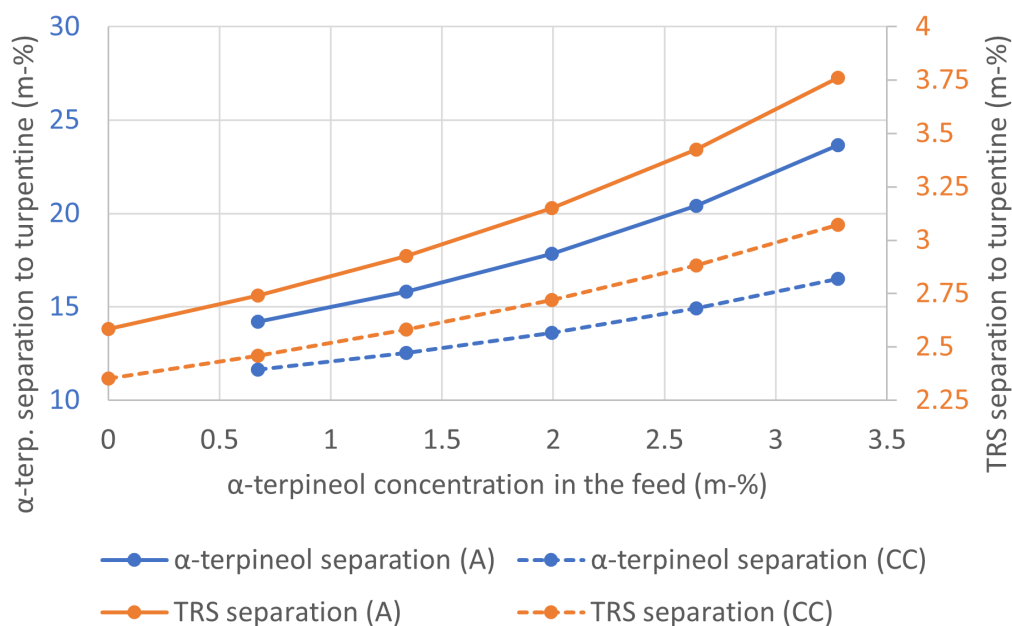


Figure 23: Sensitivity analysis on the effect of α -terpineol concentration in the feed on the separation efficiency of TRS and α -terpineol in the first decanter.

The separation of α -terpineol in the decanter was 22 to 43 % higher in Aspen compared to CHEMCAD, even though both programs used UNIFAC as the thermodynamic model. Similar differences were found in TRS separation in the decanter where the separation was 10 to 19 % higher in Aspen.

The addition of guaiacol did not cause any notable changes in the results. In all of the cases, around 95 m-% of the compound remained in the bottom product of methanol column while the rest evaporated into the distillate.

5.4 Condenser temperature of the sulphur column

The temperature of the sulphur column condenser was varied between 30 and 70 °C at 5 °C intervals. Raising the temperature increased the separation of DMDS into the sulphur column distillate and, therefore, the TRS content of the methanol column distillate decreased. The separation of the other TRS compounds was not affected since they evaporated completely already at 30 °C. Figure 24 shows that more methanol evaporated into the distillate at higher temperatures which decreased its recovery into the sulphur column bottoms. Therefore, the overall methanol yield also decreased as seen in Figure 25.

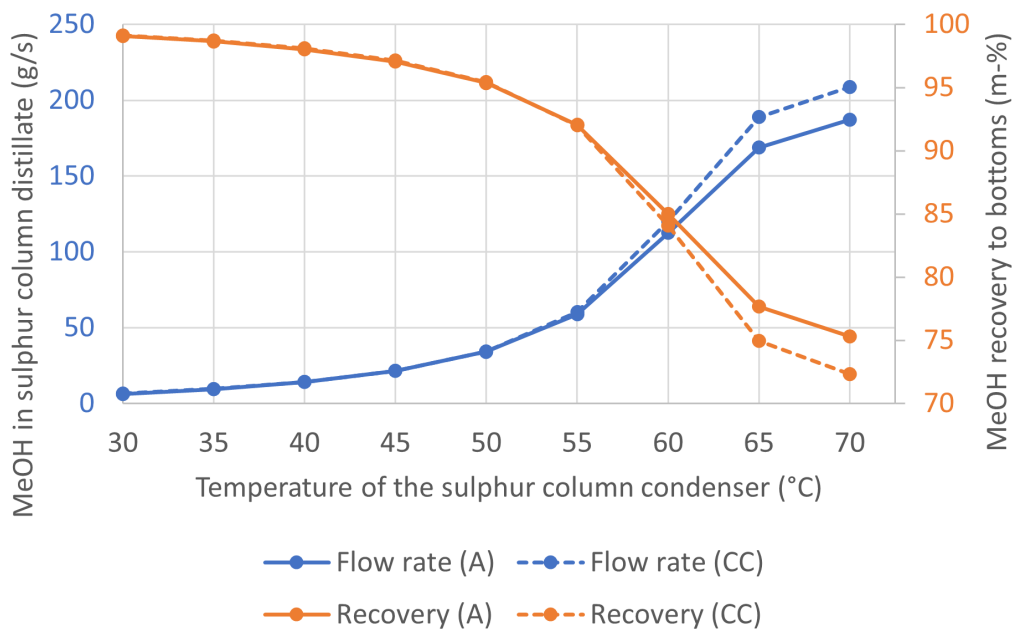


Figure 24: Sensitivity analysis on the effect of condenser temperature of the sulphur column on methanol recovery in the sulphur column.

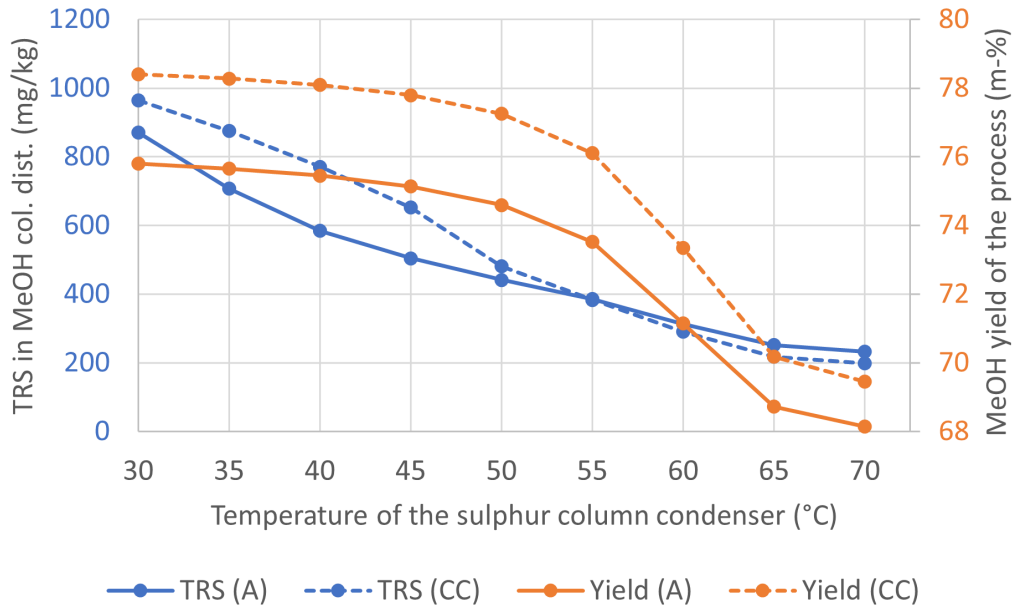


Figure 25: Sensitivity analysis on the effect of condenser temperature of the sulphur column on methanol yield and TRS concentration of the methanol column distillate.

Increasing the temperature decreased the reflux ratio due to the higher distillate rate. Consequently, the condenser duty also decreased, which is seen in Figure 26. According to the figures above, a suitable operating point could be around 45 °C

with the used feed composition. At lower temperatures, the product contains a higher amount of TRS and energy consumption is also larger. At higher temperatures, the yield starts to decline faster. In addition, the extraction process following the methanol column removes DMDS effectively, and, therefore, DMDS removal is not the main priority in the sulphur column.

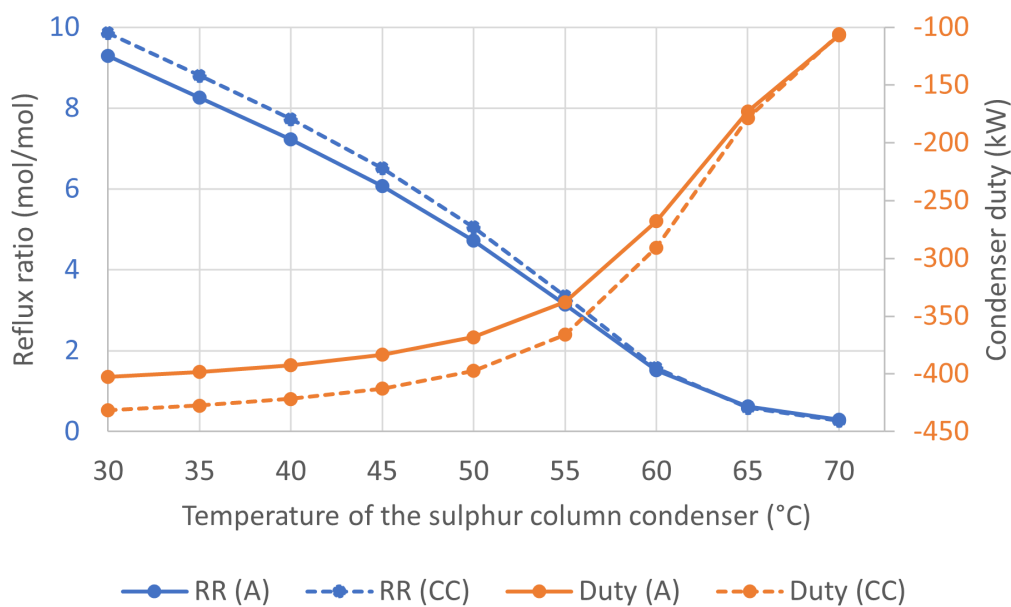


Figure 26: Sensitivity analysis on the effect of condenser temperature of the sulphur column on the reflux ratio and condenser duty in CHEMCAD and Aspen.

5.5 Steam flow into the methanol column

The low pressure steam to feed ratio into the methanol column was decreased by 75 to 25 % and increased by 25 to 100 % compared to the base case value at 25 % intervals. The temperatures of the sulphur and methanol column condensers were fixed at 45 and 63.5 °C. The effects on the methanol yield of the whole process are presented in Figure 27. Increasing the steam flow by 25 or 50 % increased the yield up to around 93 or 97 % respectively due to the higher temperature in the column. Further increases in the flow caused no changes in the yield since all methanol evaporated, and the only methanol loss occurred in the sulphur column. The increased temperature also raised the distillate rate, as shown in Figure 28. Furthermore, the distillate temperature rose by around 1 to 4 °C in the last three cases. Thus, more duty was required from the condenser to cool the product.

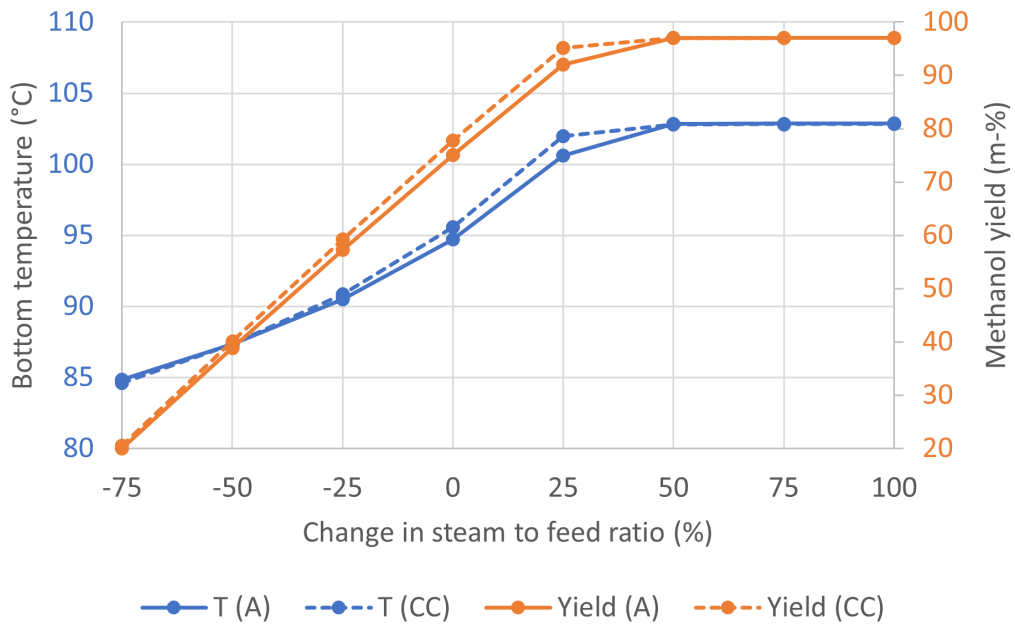


Figure 27: Sensitivity analysis on the effect of steam flow into the methanol column on the yield of the whole process.

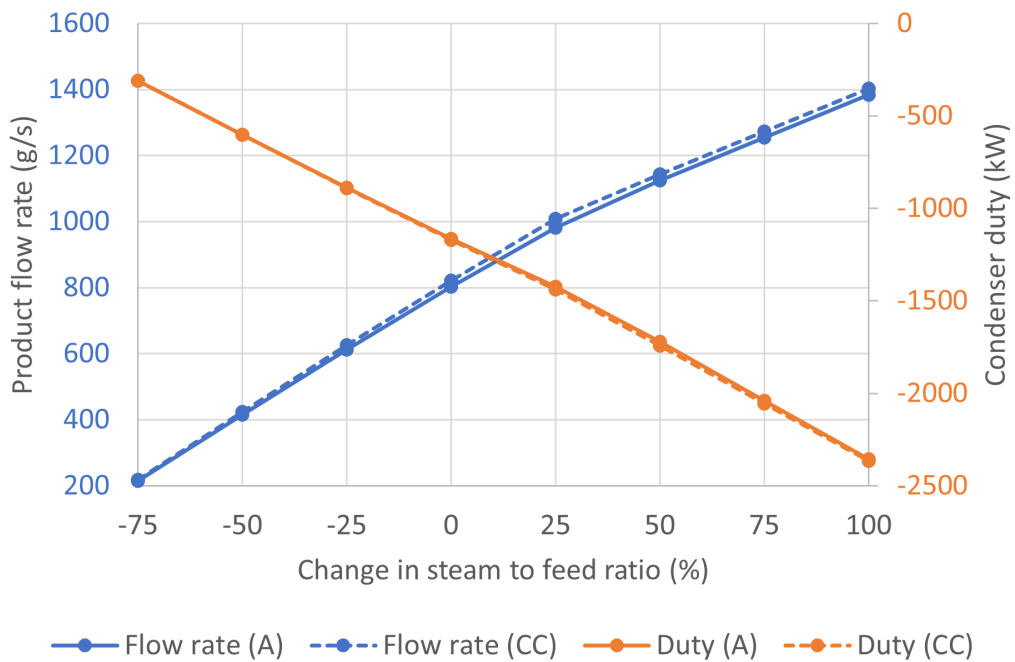


Figure 28: Sensitivity analysis on the effect of steam flow into the methanol column on the duty of the methanol column condenser.

Finally, the combined effect of the temperature of the sulphur column condenser and the steam flow into the methanol column was studied. When the steam flow was

increased by 25 to 50 m-%, methanol evaporated completely in the methanol column and the temperature of the sulphur column condenser became the only factor limiting the yield. Figure 29 shows that operating the condenser at temperatures above 50 °C caused a large decrease in the methanol yield of the process due to the loss of methanol into the sulphur column distillate. The maximum yield of around 99 m-% was achieved when the sulphur column condenser was run at 30 °C and the steam flow was increased by 50 m-% compared to the base case.

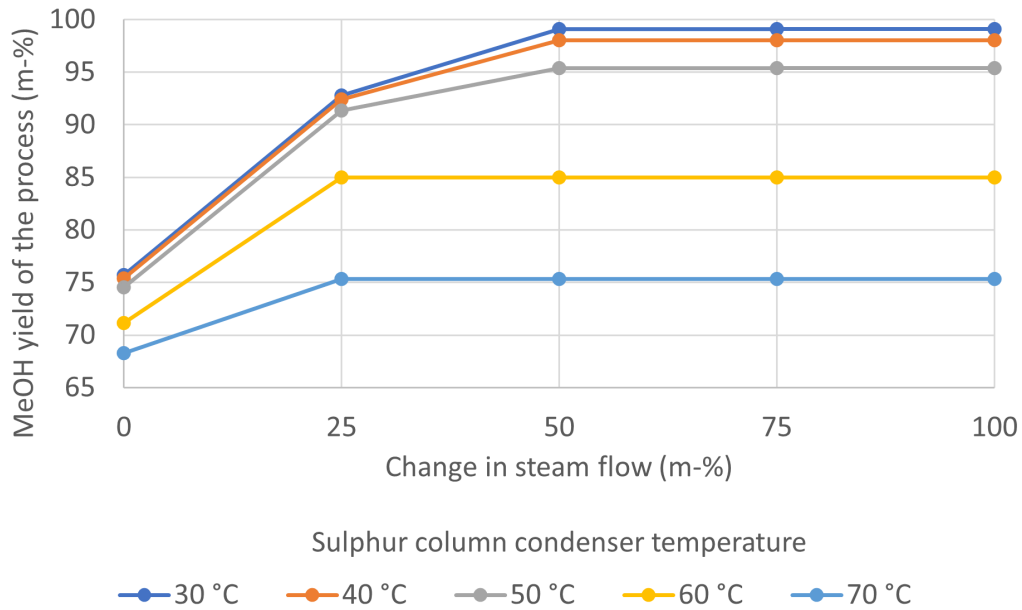


Figure 29: Sensitivity analysis on the effect of sulphur column condenser temperature and steam flow into the methanol column on the yield in Aspen Plus.

6 Conclusions and suggestions for the future

A part of the crude methanol purification process of ANDRITZ was simulated with CHEMCAD and Aspen Plus. While some differences were observed between the programs in the sensitivity analyses, the produced mass balances were very similar. Main difference was in the methanol yield which was 3.5 % higher in CHEMCAD due to the higher separation efficiency of methanol in the methanol column. The addition of BIPs for the component pairs DMS/DMDS/terpenes–water/methanol had the most notable effects on the results. Due to the formation of minimum boiling azeotropes, the volatility of DMS, DMDS and terpenes increased in the columns. Additional VLE data on water– β -pinene/3-carene/limonene systems could be useful to further improve the accuracy of the model or to validate the interactions estimated with UNIFAC. Furthermore, several BIPs were copied from one study by Olsson and Zacchi [18], and more experiments could be done to verify the consistency of their data.

In the sensitivity analyses, several operating conditions were varied and their effects were reported. It was found that, apart from DMDS, all of the TRS compounds evaporated into the sulphur column distillate at temperatures above 30 °C. Therefore, the only TRS compound in the methanol column distillate was DMDS. The optimal temperature would be between 40 and 45 °C to separate some of the DMDS but to also keep methanol yield as high as possible. The concentration of DMDS could be lowered in the MeOH column distillate by increasing the temperature of the sulphur column condenser. However, the methanol yield decreased at higher temperatures, and the steam flow into the methanol column would be required to be larger to keep the yield constant. If the goal was to reach the highest possible yield of methanol (99 %) without restricting the DMDS content, the sulphur column condenser would have to be operated at 30 °C. Additionally, the steam flow into the MeOH column would have to be raised by 50 % compared to the base case.

The main objective of this work was to improve the accuracy of the simulation. While the accuracy is difficult to assess without experimental data, the appropriate components and BIPs were added which should improve the accuracy of the simulation. It should also be mentioned that the selected components were based on crude methanol from softwood while hardwood methanol would possibly require additional compounds and BIPs. To further improve the simulation model, plant data would be required to validate the model. The accuracy of the simulation could be studied, and the need for possible new phase equilibrium experiments could be confirmed.

References

- [1] Dalena, F., Senatore, A., Marino, A., Gordano, A., Basile, M., & Basile, A. “Chapter 1 - Methanol Production and Applications: An Overview”. *Methanol*. Ed. by A. Basile & F. Dalena. Elsevier, 2018, pp. 3–28. ISBN: 978-0-444-63903-5. DOI: [10.1016/B978-0-444-63903-5.00001-7](https://doi.org/10.1016/B978-0-444-63903-5.00001-7).
- [2] Demirbaş, A. “Biodiesel from vegetable oils via transesterification in supercritical methanol”. *Energy Conversion and Management* 43(17) (2002), pp. 2349–2356. DOI: [10.1016/S0196-8904\(01\)00170-4](https://doi.org/10.1016/S0196-8904(01)00170-4).
- [3] International Renewable Energy Agency (IRENA). “Innovation Outlook: Renewable Methanol” (2021).
- [4] Bajpai, P. “12.8 Kraft Pulping”. *Biermann’s Handbook of Pulp and Paper - Raw Material and Pulp Making, Volume 1 and 2 (3rd Edition)*. Elsevier, 2018. ISBN: 978-0-12-814240-0.
- [5] Hamaguchi, M., Cardoso, M., & Vakkilainen, E. “Alternative Technologies for Biofuels Production in Kraft Pulp Mills—Potential and Prospects”. *Energies* 53390 (2012), pp. 2288–2309. DOI: [10.3390/en5072288](https://doi.org/10.3390/en5072288).
- [6] Hart, P. W. “4.10 Treatment of Contaminated Condensates”. *Chemical Recovery in the Alkaline Pulping Processes (4th Edition)*. TAPPI, 2022. ISBN: 978-1-59510-322-2.
- [7] Cheremisinoff, N. P. “Total Reduced Sulfurs”. *Pollution Control Handbook for Oil and Gas Engineering*. John Wiley & Sons, 2016. ISBN: 978-1-119-11761-2.
- [8] Zhu, J., Yoon, S.-H., Liu, P.-H., & Chai, X.-S. “Methanol formation during alkaline wood pulping”. *TAPPI Journal* 83 (2000).
- [9] Belgacem, M. N. & Gandini, A. “2.2 Turpentine”. *Monomers, Polymers and Composites from Renewable Resources*. Elsevier, 2008. ISBN: 978-0-08-045316-3.
- [10] Stenius, P. *Forest Products Chemistry*. Forest Products Chemistry bk. 3. Finnish Paper Engineers’ Association & TAPPI, 2000. ISBN: 9789525216035.
- [11] Järvensivu, M., Mäenpää, T., Jämsä-Jounela, S.-L., & Saari, K. “Field survey of reduced-sulfur emissions from a modern finnish pulp mill”. *Environmental Progress* 19(3) (2000), pp. 147–156. DOI: [10.1002/ep.670190307](https://doi.org/10.1002/ep.670190307).
- [12] Valmet. “Methanol, from waste byproduct to valuable fuel” (2018).
- [13] Lundberg, A. & Richmond, P. “The basics of foul condensate stripping” (2007).
- [14] Warnqvist, J., Släger, J. O., & Eliasson, A. *Process for removal of sulphur from raw methanol*. US Patent 10,160,706. 2018.
- [15] Niemelä, K. “Sulfur and nitrogen compounds in rectified methanol from foul condensate stripping”. *PAPTAC/TAPPI International Chemical Recovery Conference Proceedings, Charleston, South Carolina*. 2004.

- [16] “Terpenes: Importance, General Structure, and Biosynthesis”. *Terpenes*. John Wiley & Sons, Ltd, 2006. Chap. 1, pp. 1–9. ISBN: 9783527609949. DOI: [10.1002/9783527609949.ch1](https://doi.org/10.1002/9783527609949.ch1).
- [17] Gscheidmeier, M. & Fleig, H. “Turpentine”. *Ullmann’s Encyclopedia of Industrial Chemistry*. John Wiley & Sons, Ltd, 2000. ISBN: 9783527306732. DOI: [10.1002/14356007.a27_267](https://doi.org/10.1002/14356007.a27_267).
- [18] Olsson, J. & Zacchi, G. “Vapour-liquid equilibria for kraft mill condensates”. *Journal of pulp and paper science* 27(5) (2001), pp. 158–164.
- [19] Southwell, I. “Eucalyptus leaf oils: Use, chemistry, distillation and marketing”. *Phytochemistry* 31 (1992). DOI: [10.1016/0031-9422\(92\)80403-2](https://doi.org/10.1016/0031-9422(92)80403-2).
- [20] Fengel, D. & Wegener, G. *Wood: chemistry, ultrastructure, reactions*. De Gruyter, 1989, pp. 184–186. ISBN: 3-11-012059-3.
- [21] Sales, A., Felipe, L. d. O., & Bicas, J. L. “Production, properties, and applications of α -terpineol”. *Food and bioprocess technology* 13(8) (2020), pp. 1261–1279.
- [22] Wennberg, O., Saitton, D. B., & Nordlander, T. *A method and a system for obtaining methanol from foul condensate of a pulping process*. US Patent App. 16/973,196. 2021.
- [23] Der, B. & Jensen, A. S. *Methanol purification method and apparatus*. US Patent 9,320,986. 2016.
- [24] Jemaa, N. & Paleologou, M. *Method for producing bio-methanol at pulp mills*. US Patent 9,394,220. 2016.
- [25] Jensen, A., Ip, T., & Percy, J. “Methanol purification system”. *2012 TAPPI PEERS Conference, Savannah*. 2012, p. 1245.
- [26] Kenig, E. Y. & Blagov, S. “Chapter 10 - Modeling of Distillation Processes”. *Distillation*. Ed. by A. Górak & E. Sorensen. Boston: Academic Press, 2014, pp. 383–436. ISBN: 978-0-12-386547-2. DOI: [10.1016/B978-0-12-386547-2.00010-7](https://doi.org/10.1016/B978-0-12-386547-2.00010-7).
- [27] Al-Malah, K. I. M. *Aspen Plus® - Chemical Engineering Applications (2nd Edition)*. John Wiley & Sons, 2023. ISBN: 978-1-119-86869-9.
- [28] Renon, H. & Prausnitz, J. M. “Local compositions in thermodynamic excess functions for liquid mixtures”. *AIChE Journal* 14(1) (1968), pp. 135–144. DOI: [10.1002/aic.690140124](https://doi.org/10.1002/aic.690140124).
- [29] Abrams, D. S. & Prausnitz, J. M. “Statistical thermodynamics of liquid mixtures: A new expression for the excess Gibbs energy of partly or completely miscible systems”. *AIChE Journal* 21(1) (1975), pp. 116–128. DOI: [10.1002/aic.690210115](https://doi.org/10.1002/aic.690210115).
- [30] Farajnezhad, A., Afshar, O. A., Khansary, M. A., Shirazian, S., & Ghadiri, M. “Correlation of interaction parameters in Wilson, NRTL and UNIQUAC models using theoretical methods”. *Fluid Phase Equilibria* 417 (2016), pp. 181–186. DOI: [10.1016/j.fluid.2016.02.041](https://doi.org/10.1016/j.fluid.2016.02.041).

- [31] Schaschke, C. *Dictionary of Chemical Engineering*. Oxford University Press, 2014, p. 87. ISBN: 978-0-19-965145-0.
- [32] Falcimaigne, J. & Decarre, S. “1.3.5.2 Thermodynamic Models for Fluid Property Calculation”. *Multiphase Production - Pipeline Transport, Pumping and Metering*. Editions Technip, 2008. ISBN: 978-2-7108-0913-5.
- [33] Klerk, D. L. de & Schwarz, C. E. “Simplified Approach to Understanding, Evaluating, and Parameterizing the NRTL Model for the Description of Binary VLE: $\tau\tau\tau$ -VLE Approach”. *Industrial & Engineering Chemistry Research* 62(27) (2023), pp. 10629–10643. DOI: [10.1021/acs.iecr.3c00576](https://doi.org/10.1021/acs.iecr.3c00576).
- [34] *Aspen Plus 12.1 User Guide*. Available at https://esupport.aspentech.com/S_Article?id=000064707. AspenTech. 2017.
- [35] *CHEMCAD User Guide*. Available at https://www.chemstations.com/content/documents/CHEMCAD_User_Guide.pdf. Chemstations. 2021.
- [36] Marcilla, A., Reyes-Labarta, J., & Olaya, M. “Should we trust all the published LLE correlation parameters in phase equilibria? Necessity of their assessment prior to publication”. *Fluid Phase Equilibria* 433 (2017), pp. 243–252. DOI: [10.1016/j.fluid.2016.11.009](https://doi.org/10.1016/j.fluid.2016.11.009).
- [37] Fredenslund, A., Jones, R. L., & Prausnitz, J. M. “Group-contribution estimation of activity coefficients in nonideal liquid mixtures”. *AIChE Journal* 21(6) (1975), pp. 1086–1099. DOI: [10.1002/aic.690210607](https://doi.org/10.1002/aic.690210607).
- [38] Gmehling, J. & Möllmann, C. “Synthesis of Distillation Processes Using Thermodynamic Models and the Dortmund Data Bank”. *Industrial & Engineering Chemistry Research* 37(8) (1998), pp. 3112–3123. DOI: [10.1021/ie970782d](https://doi.org/10.1021/ie970782d).
- [39] Chemistry LibreTexts. *Henry’s Law*. URL: <https://chem.libretexts.org/@go/page/1599> (Accessed 11/03/2024).
- [40] Yee Foo, D. C., Chemmangattuvalappil, N., Ng, D. K. S., Elyas, R., Chen, C.-L., Elms, R. D., et al. “1.4.1 Sequential Modular Approach”. *Chemical Engineering Process Simulation*. Elsevier, 2017. ISBN: 978-0-12-803782-9.
- [41] Chen, W.-L., Hsu, C.-C., & Lin, S.-T. “Prediction of phase behaviors of acetic acid containing fluids”. *Fluid Phase Equilibria* 353 (2013), pp. 61–68. DOI: [10.1016/j.fluid.2013.05.039](https://doi.org/10.1016/j.fluid.2013.05.039).
- [42] Towler, G. & Sinnott, R. “4.5 Simulation of Unit Operations”. *Chemical Engineering Design - Principles, Practice and Economics of Plant and Process Design (3rd Edition)*. Elsevier, 2022. ISBN: 978-0-12-821179-3.
- [43] *Process Simulation Essentials*. Available at https://www.chemstations.com/content/CHEMCAD_Essentials_example_book_2021.pdf. Chemstations. 2021.

- [44] Shen, Z., Qu, Q., Chen, M., Lyu, H., & Sun, J. “Advancements in methanol distillation system: A comprehensive overview”. *Chemical Engineering Research and Design* 199 (2023), pp. 130–151. DOI: [10.1016/j.cherd.2023.09.026](https://doi.org/10.1016/j.cherd.2023.09.026).
- [45] Kuosa, M., Pokki, J.-P., Jaakkola, H., Berg, C.-G., & Kultanen, M.-L. “CHEMICAL PULPING: Modeling vapor – liquid equilibria of kraft pulp mill condensates containing methanol, turpentine and total reduced sulphur (TRS) components”. *Nordic Pulp & Paper Research Journal* 27(5) (2012), pp. 900–909. DOI: [10.3183/npprj-2012-27-05-p900-909](https://doi.org/10.3183/npprj-2012-27-05-p900-909).
- [46] Chalov, N., Goryachikh, E., & Vodolazova, L. K. “Study of the liquid–vapor compositions in binary solutions of phenol”. *Gidroliznaya I Lesokhimicheskaya Promyshlennost* 8 (1955), pp. 11–12.
- [47] Cesari, L., Namysl, S., Canabady-Rochelle, L., & Mutelet, F. “Phase equilibria of phenolic compounds in water or ethanol”. *Fluid Phase Equilibria* 453 (2017), pp. 58–66. DOI: [10.1016/j.fluid.2017.09.008](https://doi.org/10.1016/j.fluid.2017.09.008).
- [48] Zanghelini, G., Athès, V., Esteban-Decloux, M., Giampaoli, P., & Vitu, S. “Isobaric vapour-liquid equilibrium of α -terpineol highly diluted in hydroalcoholic mixtures at 101.3 kPa: Experimental measurements and thermodynamic modeling”. *The Journal of Chemical Thermodynamics* 171 (2022). Article 106806. DOI: [10.1016/j.jct.2022.106806](https://doi.org/10.1016/j.jct.2022.106806).
- [49] Tamura, K. & Li, H. “Mutual Solubilities of Terpene in Methanol and Water and Their Multicomponent Liquid-Liquid Equilibria”. *Journal of Chemical & Engineering Data* 50(6) (2005), pp. 2013–2018. DOI: [10.1021/je0502391](https://doi.org/10.1021/je0502391).
- [50] Deterre, S., Albet, J., Joulia, X., Baudouin, O., Giampaoli, P., Decloux, M., et al. “Vapor–Liquid Equilibria Measurements of Bitter Orange Aroma Compounds Highly Diluted in Boiling Hydro-Alcoholic Solutions at 101.3 kPa”. *Journal of Chemical & Engineering Data* 57(12) (2012), pp. 3344–3356. DOI: [10.1021/je3004854](https://doi.org/10.1021/je3004854).
- [51] Yu, Q., Liu, D., Liu, R., Zhou, H., Chen, M., Chen, G., et al. “VLE of H₂S-H₂O system”. *Chemical Engineering (China)* 4 (1980).
- [52] Gillespie, P. C. & Wilson, G. M. “GPA Research Report RR-48”. *Gas Processors Association, Tulsa* (1982).
- [53] Gillespie, P. C. & Wilson, G. M. *Sulfur Compounds and Water VLE and Mutual Solubility: MESH-H₂O; ETSH-H₂O; CS₂-H₂O; and COS-H₂O*. Gas Processors Association, 1984.
- [54] Kilner, J., McBain, S. E., & Roffey, M. G. “(Vapour+liquid) equilibria of (methanethiol or ethanethiol or propan-1-thiol or butan-1-thiol+ n-hexane or n-decane or toluene or water) for mole fractions $x = 0$ to 0.2 of thiol at temperatures between 323 and 373 K”. *The Journal of Chemical Thermodynamics* 22(2) (1990), pp. 203–210. DOI: [10.1016/0021-9614\(90\)90084-4](https://doi.org/10.1016/0021-9614(90)90084-4).

- [55] Jou, F.-Y., Mather, A., Schubert, C., & Schmidt, K. “Vapour–liquid equilibria in the system methanethiol–water”. *The Journal of Chemical Thermodynamics* 160 (2021). Article 106480. DOI: [10.1016/j.jct.2021.106480](https://doi.org/10.1016/j.jct.2021.106480).
- [56] Awan, J. A., Tsivintzelis, I., Breil, M. P., Coquelet, C., Richon, D., & Kontogeorgis, G. M. “Phase Equilibria of Mixtures Containing Organic Sulfur Species (OSS) and Water/Hydrocarbons: VLE Measurements and Modeling Using the Cubic-Plus-Association Equation of State”. *Industrial & Engineering Chemistry Research* 49(24) (2010), pp. 12718–12725. DOI: [10.1021/ie101470b](https://doi.org/10.1021/ie101470b).
- [57] Giles, N. F. & Wilson, G. M. “Liquid-Liquid Equilibria on Three Binary Systems: Methyl Cyclopropanecarboxalate + Water; Dimethyl Sulfide + Water; and Dimethyl Disulfide + Water”. *Journal of Chemical & Engineering Data* 51(6) (2006), pp. 1963–1965. DOI: [10.1021/je050326t](https://doi.org/10.1021/je050326t).
- [58] Kojima, K. “Determination of vapor-liquid equilibrium from boiling point curve”. *Kagaku Kougaku Ronbunshu* 32(2) (1968), pp. 149–153.
- [59] Koner, Z., Phutela, R. C., & Fenby, D. V. “Determination of the equilibrium constants of water-methanol deuterium exchange reactions from vapour pressure measurements”. *Australian Journal of Chemistry* 33(1) (1980), pp. 9–13. DOI: [10.1071/CH9800009](https://doi.org/10.1071/CH9800009).
- [60] Rieder, R. M. & Thompson, A. R. “Vapor-Liquid Equilibria Measured by a Gillespie Still - Ethyl Alcohol - Water System”. *Industrial & Engineering Chemistry* 41(12) (1949), pp. 2905–2908. DOI: [10.1021/ie50480a060](https://doi.org/10.1021/ie50480a060).
- [61] Kurihara, K., Minoura, T., Takeda, K., & Kojima, K. “Isothermal Vapor-Liquid Equilibria for Methanol + Ethanol + Water, Methanol + Water, and Ethanol + Water”. *Journal of Chemical & Engineering Data* 40(3) (1995), pp. 679–684. DOI: [10.1021/je00019a033](https://doi.org/10.1021/je00019a033).
- [62] Huang, R., Gu, Y., & Hou, Y. “VLE of Acetone-Water-Isobutyraldehyde System”. *Chem. Eng* 4 (1984), pp. 26–29.
- [63] Lieberwirth, I. & Schuberth, H. “Isothermal vapor-liquid phase equilibrium behavior of the acetone-water system at 35 °C”. *Chemischer Informationsdienst* 11(1) (1980).
- [64] Ochi, K. & Lu, B. C.-Y. “Determination and correlation of binary vapor-liquid equilibrium data”. *Fluid Phase Equilibria* 1(3) (1977), pp. 185–200. DOI: [10.1016/0378-3812\(77\)80002-2](https://doi.org/10.1016/0378-3812(77)80002-2).
- [65] Wilsak, R. A., Campbell, S. W., & Thodos, G. “Vapor—liquid equilibrium measurements for the methanol—acetone system at 372.8, 397.7 and 422.6 K”. *Fluid phase equilibria* 28(1) (1986), pp. 13–37. DOI: [10.1016/0378-3812\(86\)85066-X](https://doi.org/10.1016/0378-3812(86)85066-X).

- [66] Campbell, S. W., Wilsak, R. A., & Thodos, G. "Vapor-liquid equilibrium measurements for the ethanol-acetone system at 372.7, 397.7, and 422.6 K". *Journal of Chemical and Engineering Data* 32(3) (1987), pp. 357–362. DOI: [10.1021/je00049a021](https://doi.org/10.1021/je00049a021).
- [67] Chen, S., Bao, Z., Lü, Z., Yang, Y., Xu, W., Chen, Z., et al. "Vapor–Liquid Equilibrium for the 1, 1, 1-Trifluorotrchloroethane+ Sulfuryl Chloride System at 101.3 kPa". *Journal of Chemical & Engineering Data* 59(1) (2014), pp. 16–21. DOI: [10.1021/je400544h](https://doi.org/10.1021/je400544h).
- [68] Sapei, E., Uusi-Kyyny, P., Pokki, J.-P., Pakkanen, M., Keskinen, K. I., & Alopaeus, V. "Vapor–liquid equilibrium measurements of dimethylsulfide, +ethanol, +dimethylether, +methylacetate with a static total pressure method". *Fluid Phase Equilibria* 355 (2013), pp. 34–39. DOI: [10.1016/j.fluid.2013.06.044](https://doi.org/10.1016/j.fluid.2013.06.044).
- [69] Ben Mahdoui, N., Artigas, H., Lafuente, C., Hichri, M., & Khattech, I. "Isobaric Vapor–Liquid Equilibrium for the Binary Systems Dimethyl Disulfide + C1–C4 n-Alkanol at 40.000 and 101.325 kPa". *Journal of Chemical & Engineering Data* 62(7) (2017), pp. 2037–2043. DOI: [10.1021/acs.jced.7b00078](https://doi.org/10.1021/acs.jced.7b00078).
- [70] Mahdoui, N. B., Artal, M., Hichri, M., & Lafuente, C. "Volumetric behavior and vapor–liquid equilibrium of dimethyl disulfide+ n-alkanol binary mixtures". *Journal of Solution Chemistry* 48 (2019), pp. 1–14. DOI: [10.1007/s10953-019-00841-x](https://doi.org/10.1007/s10953-019-00841-x).
- [71] Delzenne, A. "Vapor Liquid Equilibrium Data for Ternary System Methanol-Ethanol-Water." *Industrial & Engineering Chemistry Chemical and Engineering Data Series* 3(2) (1958), pp. 224–230. DOI: [10.1021/I460004A010](https://doi.org/10.1021/I460004A010).
- [72] Kooner, Z. & Fenby, D. "Vapour pressure study of the deuterium exchange reaction in methanol-ethanol systems: equilibrium constant determination". *Australian Journal of Chemistry* 33(9) (1980), pp. 1943–1946. DOI: [10.1071/CH9801943](https://doi.org/10.1071/CH9801943).
- [73] Leu, A.-D., Carroll, J. J., & Robinson, D. B. "The equilibrium phase properties of the methanol-hydrogen sulfide binary system". *Fluid Phase Equilibria* 72 (1992), pp. 163–172. DOI: [10.1016/0378-3812\(92\)85024-3](https://doi.org/10.1016/0378-3812(92)85024-3).
- [74] Jackowski, A. W. "Vapor-liquid equilibria in binaries composed of methanol, methanethiol, and 2-thiapropane". *ChemInform* 12 (1981).
- [75] Kim, J. & Rousseau, R. "Vapor-liquid equilibria for mixtures of methanol and methyl mercaptan". *AIChE Symposium Series*. Vol. 81. 244. 1985, p. 74.
- [76] Mullins, S., Oehlert, L., Wileman, K., & Manley, D. "Experimental Vapor Liquid Equilibria for the Methanol/Dimethylsulfide, Methanol/Methyl tert-Butyl Ether, and n-Hexane/n, n-Diethylmethylamine Systems". *AIChE Symp. Ser.* Vol. 85. 271. 1989, pp. 94–101.

- [77] Cunningham, J. R. & Jones, D. K. “Experimental results for phase equilibria and pure component properties”. 1991.
- [78] Guilbot, P., Fischer, K., Valtz, A., Théveneau, P., Baba-Ahmed, A., & Richon, D. “Measurement of VLE (TP_x or TP_{xy} data) for hydrogen sulfide+(dimethylsulfide or ethylmethylsulfide or carbon disulfide) and methane solubilities in (dimethylsulfide or ethylmethylsulfide or methylmercaptan or ethylmercaptan)”. *Fluid Phase Equilibria* 260(1) (2007), pp. 49–59. DOI: [10.1016/j.fluid.2007.07.013](https://doi.org/10.1016/j.fluid.2007.07.013).
- [79] Lee, J. I., Mather, A. E., & Otto, F. D. “Vapor-liquid equilibria in the system hydrogen sulfide-methanethiol”. *Journal of Chemical & Engineering Data* 23(1) (1978), pp. 78–79. DOI: [10.1021/je60076a015](https://doi.org/10.1021/je60076a015).
- [80] Puentes, C., Joulia, X., Athès, V., & Esteban-Decloux, M. “Review and Thermodynamic Modeling with NRTL Model of Vapor–Liquid Equilibria (VLE) of Aroma Compounds Highly Diluted in Ethanol–Water Mixtures at 101.3 kPa”. *Industrial & Engineering Chemistry Research* 57(10) (2018), pp. 3443–3470. DOI: [10.1021/acs.iecr.7b03857](https://doi.org/10.1021/acs.iecr.7b03857).
- [81] Tamura, K., Li, X., & Li, H. “Temperature dependence on mutual solubility of binary (methanol + limonene) mixture and (liquid + liquid) equilibria of ternary (methanol + ethanol + limonene) mixture”. *The Journal of Chemical Thermodynamics* 41(4) (2009), pp. 564–568. DOI: [10.1016/j.jct.2008.10.013](https://doi.org/10.1016/j.jct.2008.10.013).
- [82] Tamura, K., Li, X., & Li, H. “Temperature Dependence on Mutual Solubility Data of the Binary (Methanol + α -Pinene or β -Pinene) Systems and Ternary Liquid- Liquid Equilibria for the (Methanol + Ethanol + α -Pinene or β -Pinene) Systems”. *Journal of Chemical & Engineering Data* 53(10) (2008), pp. 2417–2421. DOI: [10.1021/je800407h](https://doi.org/10.1021/je800407h).
- [83] Li, X. & Tamura, K. “(Ternary liquid + liquid) equilibria for (water + acetone + α -Pinene, or β -Pinene, or limonene) mixtures”. *The Journal of Chemical Thermodynamics* 42(11) (2010), pp. 1400–1405. DOI: [10.1016/j.jct.2010.06.004](https://doi.org/10.1016/j.jct.2010.06.004).
- [84] Englezos, P., Kalogerakis, N., & Bishnoi, P. “Simultaneous regression of binary VLE and VLLE data”. *Fluid Phase Equilibria* 61(1) (1990), pp. 1–15. DOI: [10.1016/0378-3812\(90\)90001-4](https://doi.org/10.1016/0378-3812(90)90001-4).
- [85] Selleck, F. T., Carmichael, L. T., & Sage, B. H. “Phase Behavior in the Hydrogen Sulfide-Water System”. *Industrial & Engineering Chemistry* 44(9) (1952), pp. 2219–2226. DOI: [10.1021/ie50513a064](https://doi.org/10.1021/ie50513a064).
- [86] Carroll, J. J. & Mather, A. E. “Phase equilibrium in the system water-hydrogen sulphide: Experimental determination of the LLV locus”. *The Canadian Journal of Chemical Engineering* 67(3) (1989), pp. 468–470. DOI: [10.1002/cjce.5450670318](https://doi.org/10.1002/cjce.5450670318).

- [87] Marcilla, A., Olaya, M. M., & Serrano, M. D. “Liquid-Vapor Equilibrium Data Correlation: Part I. Pitfalls and Some Ideas to Overcome Them”. *Industrial & Engineering Chemistry Research* 50(7) (2011), pp. 4077–4085. DOI: [10.1021/ie101909d](https://doi.org/10.1021/ie101909d).
- [88] Marcilla, A., Olaya, M., & Reyes-Labarta, J. “Simultaneous VLE data correlation for ternary systems: Modification of the NRTL equation for improved calculations”. *Fluid Phase Equilibria* 426 (2016), pp. 47–55. DOI: [10.1016/j.fluid.2015.12.047](https://doi.org/10.1016/j.fluid.2015.12.047).
- [89] Kleiber, M. *Process Engineering: Addressing the Gap between Study and Chemical Industry*. De Gruyter, 2020, p. 79. ISBN: 9783110657685.
- [90] Weidlich, U. & Gmehling, J. “A modified UNIFAC model. 1. Prediction of VLE, hE, and γ^∞ ”. *Industrial & Engineering Chemistry Research* 26 (1987), pp. 1372–1381. DOI: [10.1021/IE00067A018](https://doi.org/10.1021/IE00067A018).
- [91] The UNIFAC Consortium. *Model Comparison*. URL: <https://unifac.ddbst.com/model-comparison.html> (Accessed 19/02/2024).
- [92] Klamt, A. “Conductor-like screening model for real solvents: a new approach to the quantitative calculation of solvation phenomena”. *The Journal of Physical Chemistry* 99(7) (1995), pp. 2224–2235. DOI: [10.1021/j100007a062](https://doi.org/10.1021/j100007a062).
- [93] Klamt, A. & Eckert, F. “COSMO-RS: a novel and efficient method for the a priori prediction of thermophysical data of liquids”. *Fluid Phase Equilibria* 172(1) (2000), pp. 43–72. DOI: [10.1016/S0378-3812\(00\)00357-5](https://doi.org/10.1016/S0378-3812(00)00357-5).
- [94] Klamt, A., Eckert, F., & Arlt, W. “COSMO-RS: an alternative to simulation for calculating thermodynamic properties of liquid mixtures”. *Annual review of chemical and biomolecular engineering* 1 (2010), pp. 101–122. DOI: [10.1146/annurev-chembioeng-073009-100903](https://doi.org/10.1146/annurev-chembioeng-073009-100903).
- [95] Felton, K. C., Ben-Safar, H., & Alexei, A. “DeepGamma: A deep learning model for activity coefficient prediction”. *1st Annual AAAI Workshop on AI to Accelerate Science and Engineering (AI2ASE)*. 2022.
- [96] Sun, G., Zhao, Z., Sun, S., Ma, Y., Li, H., & Gao, X. “Vapor-liquid phase equilibria behavior prediction of binary mixtures using machine learning”. *Chemical Engineering Science* 282 (2023). Article 119358. DOI: [10.1016/j.ces.2023.119358](https://doi.org/10.1016/j.ces.2023.119358).
- [97] Winter, B., Winter, C., Esper, T., Schilling, J., & Bardow, A. “SPT-NRTL: A physics-guided machine learning model to predict thermodynamically consistent activity coefficients”. *Fluid Phase Equilibria* 568 (2023). Article 113731. DOI: [10.1016/j.fluid.2023.113731](https://doi.org/10.1016/j.fluid.2023.113731).
- [98] National Center for Biotechnology Information. *PubChem Compound Summary for CID 6097028, Ammonium Sulfate*. URL: <https://pubchem.ncbi.nlm.nih.gov/compound/Ammonium-Sulfate> (Accessed 22/02/2024).

- [99] Hemptinne de, J.-C., Ledanois, J.-M., Mougin, P., & Barreau, A. “3.4.2.5 Electrolyte Models”. *Select Thermodynamic Models for Process Simulation - A Practical Guide Using a Three Steps Methodology*. Editions Technip, 2012. ISBN: 978-2-7108-0949-4.
- [100] Gmehling, J., Kleiber, M., Kolbe, B., & Rarey, J. “7.3 Activity Coefficient Models for Electrolyte Solutions”. *Chemical Thermodynamics for Process Simulation (2nd Completely Revised and Enlarged Edition)*. John Wiley & Sons, 2019. ISBN: 978-3-527-34325-6.
- [101] Hyndman, R. J. & Koehler, A. B. “Another look at measures of forecast accuracy”. *International Journal of Forecasting* (4) (2006), pp. 679–688. DOI: [10.1016/j.ijforecast.2006.03.001](https://doi.org/10.1016/j.ijforecast.2006.03.001).

B Phase equilibrium diagrams

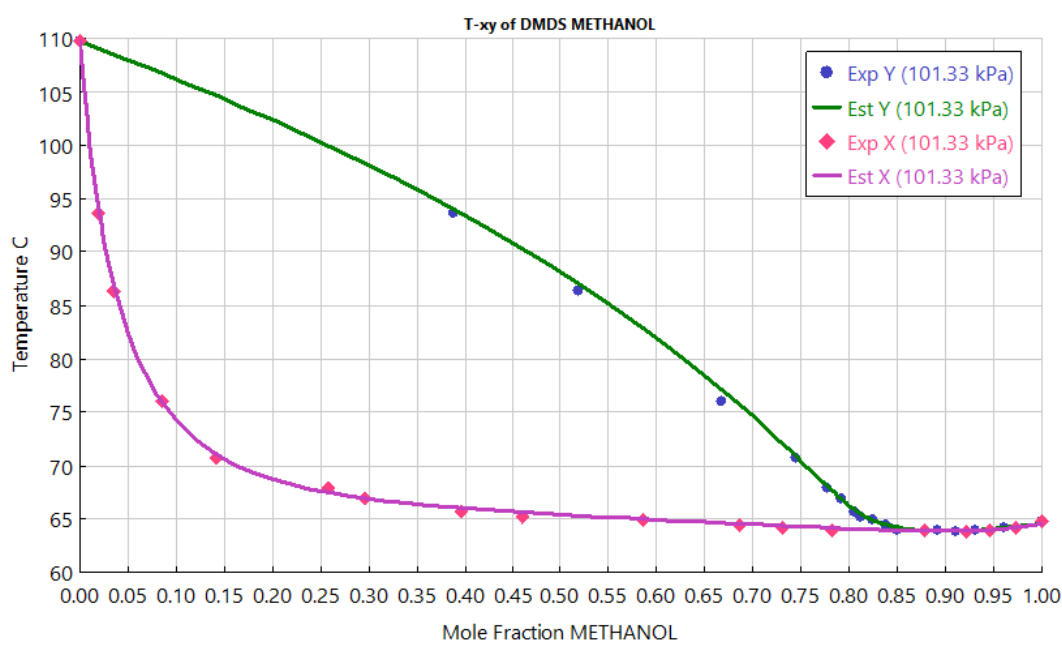


Figure B1: Txy diagram of methanol–DMDS with regressed BIPs compared to experimental data from Mahdoui et al. [69].

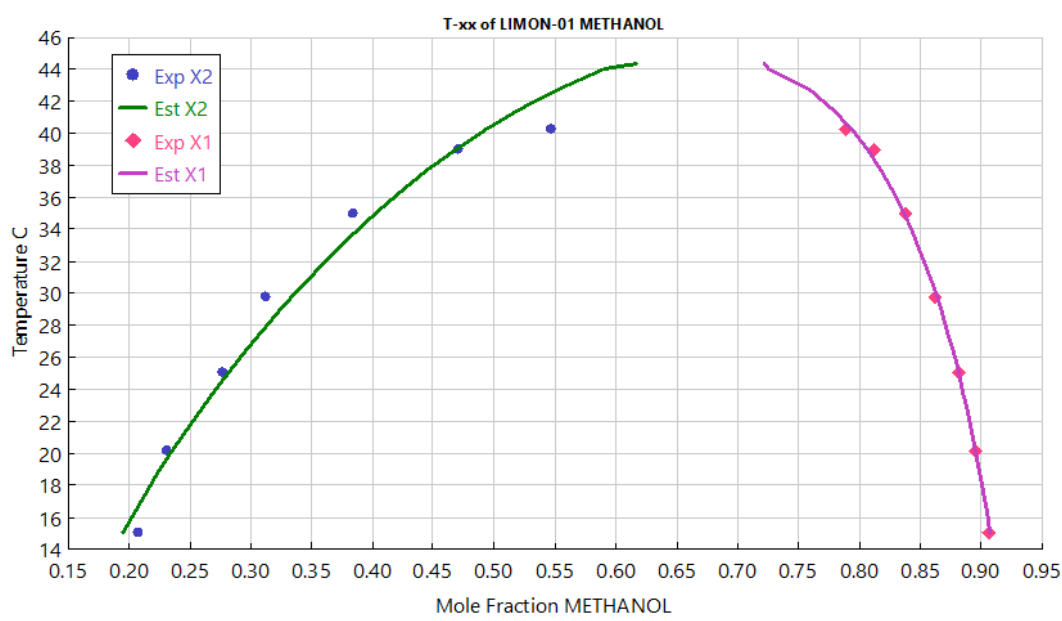


Figure B2: Txx diagram of methanol–limonene with regressed BIPs compared to experimental data from Tamura et al. [81].

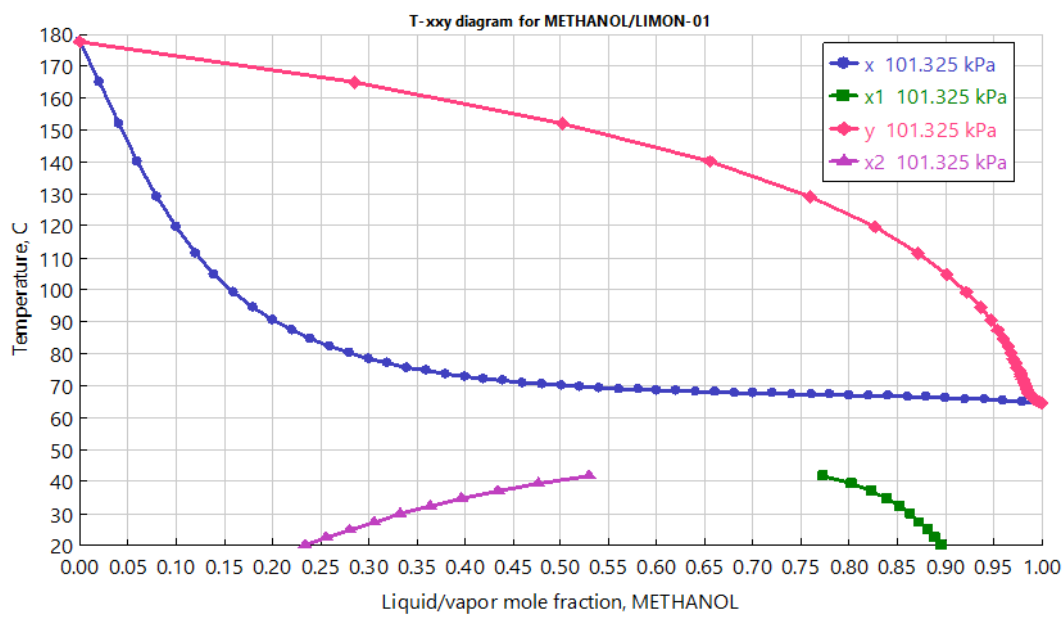


Figure B3: Txy diagram of methanol–limonene with regressed BIPs.

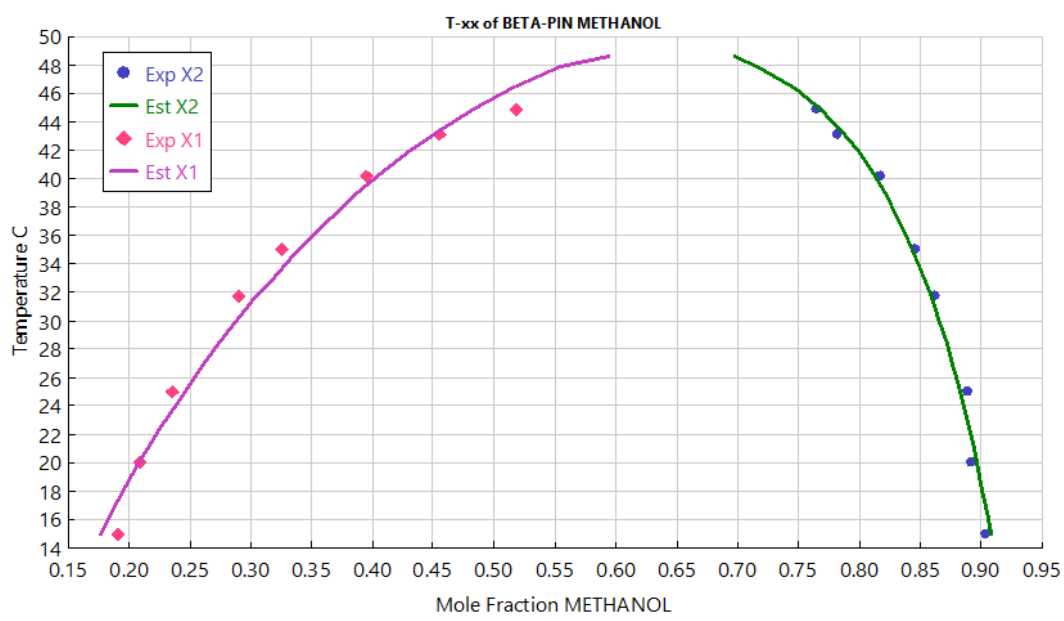


Figure B4: Txx diagram of methanol– β -pinene with regressed BIPs compared to experimental data from Tamura et al. [82].

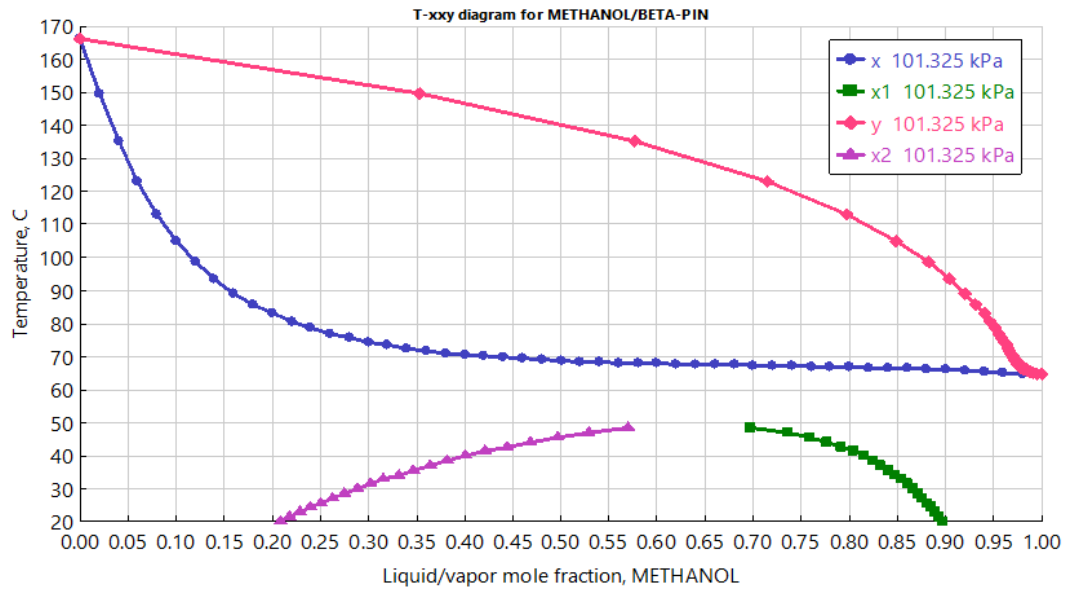


Figure B5: Txy diagram of methanol– β -pinene with regressed BIPs.

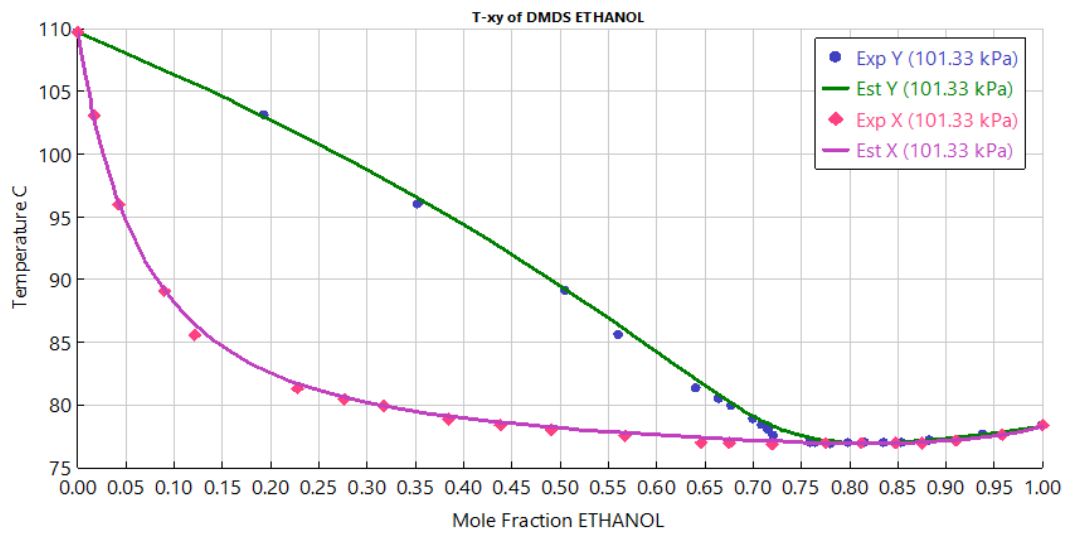


Figure B6: Txy diagram of ethanol–DMDS with regressed BIPs compared to experimental data from Mahdoui et al. [69].